Student thesis series INES nr 581

Snow-graupel collisions in clouds: a newly derived formulation for breakup of single crystals

Victor Craig van der Brug

2022
Department of
Physical Geography and Ecosystem Science
Lund University
Sölvegatan 12
S-223 62 Lund
Sweden

Victor Craig van der Brug (2022).
Snow-graupel collisions in clouds: a newly derived formulation for Breakup of single crystals
Snö-graupel-kollisioner i moln: en nyligen härledd formulering för uppdelning av enkristaller
Master degree thesis, 30 credits in *Atmospheric Science & Biogeochemical Cycles*
Department of Physical Geography and Ecosystem Science, Lund University

Level: Master of Science (MSc)

Course duration:

Disclaimer

Snow-graupel collisions in clouds: a newly derived formulation for breakup of single crystals

---

Victor Craig van der Brug

Master thesis, 30 credits, in *Atmospheric Science & Biogeochemical Cycles*

Vaughan Phillips
Department of Physical Geography and Ecosystem Science, Lund University

Marcin Jackowicz-Korczynski
Department of Physical Geography and Ecosystem Science, Lund University

Exam committee:

Thomas Holst
Department of Physical Geography and Ecosystem Science, Lund University

Sachin Patade
Department of Physical Geography and Ecosystem Science, Lund University

Acknowledgements

Vaughan Phillips, for his advice, insight, and knowledge on the subject matter.

Marcin Jackowicz-Korczynski, for providing his laboratories and equipment across borders.

Martin & Biep van der Brug, for their devotion and patience.

Mink's IJs, the ice cream parlour for providing the freezer necessary to keep the research going.

Gerard van der Zwet, for advice and guidance.

Abstract

The observed and well-known discrepancy between concentrations of ice nucleating particles in the environment and the concentrations of ice particles in clouds show that there are additional 'secondary' processes enhancing the concentrations of ice particles. In present-day modelling of weather and climate, such processes are mostly overlooked and thus a cause for uncertainty.

Recent modelling studies have shown that one of the secondary ice production (SIP) mechanisms can have a dominant influence in some cloud types. This mechanism is fragmentation due to collisions between ice particles in clouds. The most prolific collision type is between snow and graupel particles.

In the present project, the goal of the research was to use additional empirical evidence to improve the values of parameters in Phillips' theoretical formulation, presented by Phillips et al. (2017b), when applied to collisions between crystals and graupel/hail. This formulation is the only comprehensive model of in-cloud ice-ice collisions to date. Empirical data from inspection of a past published lab study is shown here and implemented into the theoretical scheme of Phillips formulation through combination with photographic evidence of ice particle morphology from the literature.

The newly parameterised scheme can be implemented for 5 different crystal types in the temperature range of -4 to -25°C. The results imply that fragmentation in snow-graupel collision might have a larger effect on ice multiplication than is currently modelled.

In addition, an experimental set-up was developed and used to grow graupel and snow crystal particles. Recommendations for possible future experiments to observe this process of SIP are discussed.

Table of Contents

1 Introduction

Clouds can consist of tiny water droplets, ice crystals, or both; in the third instance, they are referred to as mixed-phase clouds (MPCs). The ice concentration of clouds, especially in MPCs, has an important effect on the role of the cloud in the water cycle and its behaviour in the atmosphere. The concentration of ice in clouds influences precipitation rates through a multitude of pathways and mechanisms (Lohmann and Feichter 2005; Seinfeld et al. 2016; Phillips et al. 2017a), it also directly and indirectly influences the clouds' lifetime (Seinfeld et al. 2016; Lauber et al. 2021) and the Earth's radiative budget by reflecting incoming short-wave radiation and trapping outgoing long-wave radiation (Lohmann and Feichter 2005; Seinfeld et al. 2016).

The precipitation from clouds can fall in many shapes and forms: rain droplets, snow, hail, and the less commonly known precipitation form called graupel. Graupel particles are ice particles in which more than half the mass comes from small droplets freezing on the surface of a small snow crystal or other ice particles — a process called riming (Takahashi and Fukuta 1988). The frozen particles in a cloud eventually all stem from the initial freezing of supercooled water droplets in the atmosphere. This ice production occurs in two phases: primary ice production (PIP) and secondary ice production (SIP). PIP follows two major pathways, homogenous and heterogeneous freezing. Homogenous freezing means that the conditions are cold enough for water droplets to freeze by themselves; however, in the atmosphere, supercooled water droplets can exist up to -40°C. Between this temperature and 0°C is the domain of heterogeneous freezing, which requires the presence of an ice nucleating particle (INP) (Mossop 1985; Field et al. 2017). From the initial creation of ice in clouds, the ice particles undergo growth, or they disappear through melting or sublimation.

Throughout the 20th century, modelling efforts and in situ measurements in cold precipitating clouds led the scientific community to a consensus that the concentration of INPs could not explain the ice concentration in MPCs (Mossop 1985; Field et al. 2017; Ladino et al. 2017). This means that after PIP, other mechanisms enhance the ice concentration in clouds. Hypotheses surrounding SIP, and what it could be, started to develop because of the consensus. SIP causes ice fragments or splinters from existing particles to be initiated by mechanisms

involving existing ice particles and other particles in their surroundings, either frozen or liquid (Field et al. 2017). The most famous of the proposed SIP mechanisms is the Hallett–Mossop (HM) process, in which small ice fragments are released during riming and therefore also known as rime splintering (Mossop 1980). However, besides the process of rime splintering, an intuitively easier method was proposed in the form of ice–ice collisions. The latter occurs when two ice particles in clouds collide and fragments are ejected from the weaker particle. This mechanism may be possible in turbulent convective clouds, where there is a higher chance of two particles meeting with velocities high enough to create collisional fragmentation. Nevertheless, how intuitive this mechanism may be, there is a distinct lack of experimental research surrounding it. Vardiman (1978) and Takahashi et al. (1995) conducted experimental research into ice–ice collisions and concluded that it is possible, with peak fragmentation at -15°C. The most productive collision type in terms of fragmentation is expected to be collisions between heavily rimed graupel and snow particles (Field et al. 2017; Phillips et al. 2017b). As these were the only two known datasets and physical experiments, they are the only sources that are used as an empirical foundation for modelling efforts into this pathway. An additional dataset of collision experiments has been found in Griggs and Choularton (1986) which gives an indication of the minimum breaking strength of five snow crystal morphologies.

One modelling effort used a well-studied cloud band over the U.S. High Plains and tried to recreate it using two cloud models, including the previously excluded ice-ice collision pathway. The results showed that ice–ice collisions possibly initiated 95–98% of non-homogenous ice creation, with 60–90% of total ice particles created by snow–graupel collisions (Phillips et al. 2017a). As both the range and the impact of these numbers are rather large, the uncertainty surrounding this SIP mechanism becomes apparent. Most existing weather or cloud models only incorporate the HM process, which could limit their effectiveness by ignoring ice–ice collisions. The theoretical model used by Phillips et al. (2017b) includes parameters based on the previously mentioned experimental studies.

This research aims to increase the certainty of the parameters determined by Phillips et al. (2017b), thus allowing future studies to develop a better understanding and implementation of ice-ice collisions in microphysical processes in clouds. This will be done by looking into the relations between collision kinetic energy (CKE), temperature, and fragmentation. A better understanding of these parameters and variables and their influence on fragmentation caused

by ice-ice collisions, in turn, will improve weather forecasting and climate modelling. The goal was targeted through a two-pronged approach, the first was to see if the additional empirical data can be implemented to strengthen and develop the Phillips formulation model. The second approach was to develop an experiment into snow-graupel collisions. This collision type is hypothesized to be the most promising collision between different cloud ice types (Vardiman 1978; Phillips et al. 2017b).

This report provides a background on the initiation and role of ice concentrations and particles in clouds, with a specific focus on research efforts into ice–ice collisions. The background, or state of science, is followed by a description of the methods used and data found in this research. Afterwards, the numerical efforts into developing the Phillips formulation by the newly found empirical evidence in Griggs and Choularton (1986) will be described. The attempts at the experimental approach to create reproducible and measurable snow and graupel particles will be described. The set-up, however, requires further development to produce collisional data that will overcome the criticisms of existing experimental research, this will be further discussed in the report. A discussion of the research follows, leading to a conclusion about the uncertainty surrounding this SIP mechanism and its future in cloud microphysics academia.

2 State of science

To understand the importance of fragmentation due to snow–graupel collisions, a thorough understanding of the role of ice in clouds and the possible effectiveness of these collisions as a SIP mechanism must be understood. This chapter will provide this context by explaining the role and origin of ice in clouds. Accordingly, the scientific background of ice–ice collisions will be discussed in depth. After the background and context have been described, a detailed explanation of the research question and aim will be given.

2.1 The role of ice in clouds

When ice particles are formed in MPCs they consume water from the cloud more quickly than water droplets (Lohmann and Feichter 2005; Seinfeld et al. 2016). This greater speed is caused by the lower vapor saturation pressure over ice versus over liquid water, which leads to supercooled water droplets evaporating whereas ice particles start growing (Lohmann and Feichter 2005). This is called the Wegener–Bergeron–Findeisen process and is an important process in precipitation forming (Lohmann and Feichter 2005). As ice particles grow, they become heavy enough to fall as precipitation (Seinfeld et al. 2016). However, this is not the only effect ice particles can have in clouds, and their link to this complex system can influence multiple outcomes. To illustrate; as ice particles grow faster and thus fall sooner, precipitation can increase, which in turn decreases cloud lifetime as the water content of the cloud washes out with the increased precipitation (Seinfeld et al. 2016). Opposingly, if the Wegener-Bergeron-Findeisen can incite a rapid glaciation of the cloud, the tiny ice particles are formed rapidly and have little time to grow. Thus, these ice particles have too little mass to precipitate in updrafts and then the precipitation rate is subdued (Phillips et al. 2017a). Meaning that the influence of ice concentration on precipitation is intricate and complex, and liable to a plethora of factors in the cloud.

The effects of ice in clouds on the local and global climate are not limited to their role in the precipitation of the cloud (Seinfeld et al. 2016). Clouds form an important part of the Earth's radiative budget by reflecting incoming short-wave radiation from the sun and absorbing and re-emitting long-wave radiation emitted from the Earth's surface (Christensen 2013; Seinfeld et al. 2016). Cloud particle size and lifetime are significant determinants of the clouds'

behaviour in this role, with higher concentrations of smaller particle sizes reflect more incoming radiation (IPCC 2013; Seinfeld et al. 2016). Quick glaciation of clouds leads to high concentrations of small particles, which effectively reflect incoming short-wave radiation (IPCC 2013; Seinfeld et al. 2016). Cloud lifetime, meanwhile, determines how long a cloud can play this role (IPCC 2013; Seinfeld et al. 2016). Cloud altitude and latent heat release due to internal mechanisms such as ice formation, sublimation, and melting impact the Earth's energy and radiative budget (IPCC 2013; Seinfeld et al. 2016). The role of clouds in this complex system is the source of many issues and uncertainties in weather forecasting and climate modelling (IPCC 2013).

As discussed above, the ice in clouds affects precipitation and radiative budget. However, another important role a cloud's ice content has in the atmosphere is its impact on electrical charge structure. When graupel particles collide with smaller ice particles, a charge transfer and separation occurs (Berdeklis and List 2001). Laboratory studies have shown that graupel that undergoes sublimation gains a negative charge, whereas graupel particles that grow through deposition develop a positive charge (Williams et al. 1991). The updraft in convective clouds increases the mixing and thus interaction of ice particles with each other and with supercooled water droplets. These conditions lead to cloud electrification and possibly lightning (Guo et al. 2016). The role of graupel in this process is essential as it is hypothesized that initial electrification of thunderclouds will not commence until graupel particles with a diameter of 5 mm are present (Berdeklis and List 2001). A peak of charge transfer in these ice crystal and graupel collisions is observed around -16°C. Further studies support these findings and show that small cloud droplets and low relative humidity lead to stronger positive charges of graupel and vice versa (Avila and Pereyra 2000; Berdeklis and List 2001). The presence of graupel and ice crystals is thus important to cloud electrification and the concentration and mixing rates contribute to storm intensity (Pattnaik et al. 2011; Fuchs et al. 2015).

To summarize, the ice in clouds has significant effects on the local weather and the climate system. As the role of clouds in the climate system is relatively uncertain, a thorough understanding of cloud microphysical processes is needed to reduce uncertainty in weather and climate models.

2.2 Ice formation and origin

To develop the knowledge and understanding of cloud ice it is necessary to understand where the ice particles originate and what processes and mechanisms influence ice concentrations in clouds. As of now, there are two known production phases of ice in clouds: PIP and SIP. This section will provide an overview of the mechanisms and pathways in both ice production phases.

2.2.1 Primary ice production

Ice in clouds is initially produced by either homogeneous or heterogeneous nucleation. Homogeneous nucleation, or the spontaneous freezing of supercooled water droplets, only takes place at temperatures below -36°C (Mossop 1985; Field et al. 2017).

At temperatures above this threshold, supercooled water droplets must overcome an energy barrier to freeze. The presence of a surface to freeze upon solves this problem, and thus heterogeneous freezing at temperatures above -36°C involve INPs. INPs can enhance freezing in three different ways.

1. Deposition ice nucleation: supersaturation rate of water vapor is larger for ice than water the vapor freezes on an INP immediately. This process is expected not to have significant impacts on MPCs (Kanji et al. 2017).
2. Contact freezing: the INP touches the surface of a supercooled water droplet, either from within or from outside the droplet, affecting surface energy and causing it to freeze. The process is not well understood but could be important to MPCs (Kanji et al. 2017).
3. Immersion freezing: INPs immersed in water droplets cause the droplet to freeze. This process is deemed to be the most important for MPCs (Kanji et al. 2017). These INPs are possibly initially active as cloud condensation nuclei before becoming immersed (Kanji et al. 2017).

2.2.2 Secondary ice production

After the second world war, research into clouds increased and taking measurements in clouds through aerial measurement campaigns became a part of research methods. These campaigns, however, enabled a seemingly paradoxical observation: the concentration of INPs can be lower

than the ice crystal concentration within clouds (Koenig 1963; Harris-Hobbs and Cooper 1987; Ladino et al. 2017; Lauber et al. 2021). The ice crystal concentrations were even experimentally observed to be higher than the concentrations of INPs by an order of magnitude of 4 (Hallett and Mossop 1974). The discovery of this discrepancy led to hypotheses of other mechanisms that increase the amount of ice particles in clouds, known as SIP. During the second half of the 20th century the following mechanisms were identified and hypothesized to contribute to SIP in the atmosphere:

Fragmentation of droplets during freezing:

A cloud droplet that is freezing can have water inside the growing ice shell that forms around the droplet. As water expands when it freezes the pressure inside this shell on the liquid water grows. If that pressure grows large enough to exceed a critical point the shell may break and cause splinters to be released (Mignani et al. 2019). These splinters are then counted as SIP particles.

Hallett–Mossop mechanism:

The HM mechanism is the splintering of ice during riming, where riming is the process of supercooled water droplets freezing on a solid surface. By spinning a rod through a supercooled cloud in a cold box, Hallett and Mossop (1974) showed that splinters of ice were a side effect of the riming process. The proposed mechanism behind this is still under debate (Field et al. 2017). It is widely accepted that the HM process requires supercooled water droplets smaller than 13 μm or larger than 24 μm and within a temperature range of -3°C to -8°C (Field et al. 2017; Sullivan et al. 2018b). The HM process is the most studied and most incorporated in models out of all the known SIP mechanisms, overshadowing the other processes in both understanding and research efforts (Field et al. 2017).

Ice particle fragmentation due to droplets freezing on their surface, causing thermal shock:

During the riming of droplets on other surfaces, latent heat is released, and part of this energy will be transferred to the surface on which the droplet rimes. If this riming takes place on an ice crystal and the transferred energy is large enough, then a thermal shock in the ice crystal may create cracks and cause splintering (Field et al. 2017).

Ice particles that fragment during sublimation:

In subsaturated cloud conditions, larger ice particles may fragment when smaller pieces of rime sublimate from its surface. In situ measurements have indicated that this process is dependent on a low relative humidity over the surface of the ice particles (Field et al. 2017). For a SIP mechanism to explain the discrepancy between large concentrations of ice crystals and low number of INPs, practically water-saturated cloud conditions are required to enhance ice crystal growth. However, Deshmukh et al. (2022) provided a representation of this SIP mechanism for dendritic snow and graupel. They showed theoretically that ice concentrations may be enhanced by an order of magnitude in deep convective downdrafts (Deshmukh et al. 2022).

Activation of ice nucleating particles in transient supersaturation around freezing drops:

When a supercooled water droplet freezes its surface temperature goes up to the freezing point. In atmospheric conditions which favour cloud growth, this would mean that the atmospheric temperature is lower than the surface temperature of the droplet. As the surrounding atmospheric conditions are colder than the surface of the droplet it will release water vapor to the immediate surroundings, creating a small, supersaturated band of air around the droplet. Within this band around the freezing droplet INPs may be activated, and if the atmospheric conditions are cold enough these will form new ice particles (Field et al. 2017).

Fragmentation due to ice–ice collisions:

The process here is mechanical fragmentation due to the breakup of ice particles upon collision. There have only been two known physical experimental studies conducted into the mechanism and thus laboratory data on singular collisions is minimal (Phillips et al. 2017b). As this mechanism is the subject of this study, it will be elaborated on in section 2.3.

Field et al. (2017) stressed the need for further research in all the above-mentioned SIP mechanisms as the microphysical processes are currently not well understood. Laboratory data and methods sometimes may lead to uncertainties concerning to what extent certain processes influence cloud ice and their feasibility.

2.3 Ice–ice collisions

The following section will more deeply examine previous physical experiments in ice–ice collisions and the modelling efforts that form the basis of the experimental research of this thesis. The steps taken and described in previous studies helped shaping the methods for this research. Furthermore, criticism of these studies served to sharpen the methods used and thus forms an essential part of the literature review. The modelling efforts described in the following section affect the data analysis and emphasize the problem of implementing experimental results in larger weather and climate models.

2.3.1 Previous experiments

In a laboratory experiment, Vardiman (1978) let unrimed plane dendrites fall into a humidified cold chamber. In this cold chamber, a 1mm copper mesh was placed and the fragments from the falling snowflakes were counted. This experiment lacked velocity measurements and was thus deemed insufficient; however, the analyses of the qualitative fragmentation results led to the conclusion that mechanical breakup creates relatively large particles, noticeable by camera (Vardiman 1978). During the winter of 1973–1974 Vardiman (1978) conducted a physical experiment in in which a close-up and slow-motion camera was placed facing a black plexiglass wall that was put outside when it precipitated snow or other ice particles. The experiments were conducted on a mountain side and the experimental apparatus could be positioned in such a way that the falling cryometers always fell perpendicular to the plexiglass wall (Vardiman 1978). The film data was analysed and the number of fragments were counted (Vardiman 1978). The fragments were captured in hexane and pictures taken through a microscope were analysed to classify the types of crystals and particles that were involved in the collision. The resulting relationships between the diameter of the particle, its mass and terminal velocity observed by Vardiman (1974, 1978) or taken from previous research, are presented below in Table 1:

Table 1. Mass-diameter and terminal velocity-diameter relations from literature and observed particles combined by Vardiman (1974), the D stands for the diameter of the particle in metres.

Crystal type	**Mass-diameter equation (kg)**	**Fall velocity equation (m/s)**
Unrimed dendrites	$(3.8\times10^{-3})\times D^2$	$(8.4\times10^{-0.698})\times D^{0.217}$
Light rimed dendrites	$(2.7\times10^{-2})\times D^2$	$(9.4\times10^{-0.194})\times D^{0.301}$
Heavy rimed dendrites	$(2.7\times10^{-3})\times D^2$	$(25.5\times10^{-0.764})\times D^{0.206}$
Light rimed spatial crystals	$(1.0\times10^{-2})\times D^2$	$(25.5\times10^{-0.764})\times D^{0.206}$
Graupel	$(6.5\times10^{-5})\times D^2$	$5.61+1.38\mathrm{Log}_{10}(D)$

A similar experimental approach to the research conducted by Vardiman (1974, 1978) was a field experiment conducted by Gautam (2022). On the 24th of February 2022 in the north of Sweden, in a place called Vindeln, the snowfall of an orographic stratiform cloud was captured in an open top chamber. Ice spheres assumed to be representative of graupel in snow-graupel collisions covered the bottom of this chamber. With camera equipment measurements were taken of the fragmentation of the dendritic snow crystals observed, their size distribution, and velocities. The mass-size relations of the particles during the precipitation phase were observed with other equipment alongside the collision chamber simultaneously. The observations of mass-size relations, fall velocity-size relations are reported to correspond well with previously published studies, such as Vardiman (1974, 1978) (Gautam 2022).

Griggs and Choularton (1986) fired small glass beads with multiple sizes and velocities at different types of rime and ice crystals. The ice crystals were grown on a rod in a cold chamber and the glass beads were fired or dropped at the crystals through a tube. The goal of the experiment was to find the minimum velocity of the glass bead for which fragments would break off the ice particle (Griggs and Choularton 1986). The results of which can be seen below in Table 2:

Table 2. Minimum velocity at which air alone or a glass bead of 270 μm-diameter breaks an approximately 3mm long ice crystal upon collision (Griggs and Choularton 1986). The breaking velocity measurement with the glass bead of 270 μm diameter was unobtainable by Griggs and Choularton (1986) and is therefore extrapolated by them with data from other experiments (Griggs and Choularton 1986).

		Minimum velocities to create breakage	
Crystal type	**Temperature (°C)**	**air alone (m/s)**	**270 μm-diameter beads (m/s)**
Needles	-3 to -5	9	5 ± 50%
Prisms	-5 to -8	11	6 ± 50%
Plates	-8 to -12	11	6 ± 50%
Dendrites	-12 to -16	2	1 ± 50%
Plates	-16 to - 25	8	4 ± 50%

Based on the velocities and sizes of the glass beads, the energy which is necessary to break off rime or splinters from the targeted ice particle was calculated. The results indicated that collisions between larger graupel particles and vapour-grown ice crystals are most likely to cause fragmentation (Griggs and Choularton 1986). The study found that riming the crystal types to various degrees returned the same breakage velocity results within the error ranges. Plate crystals became weaker below -16°C as opposed to their strength when grown at temperatures above -12°C. Griggs and Choularton (1986) concluded that because of the extreme conditions and the graupel or hail sizes needed to create enough force, the ice–ice collision mechanism is not likely to create enough particles for ice multiplication in clouds.

Takahashi et al. (1995) conducted the most recent physical experiment into ice–ice collisions. Their study was inspired by observations that only small and large graupel particles were observed in winter maritime cumulus clouds over the Japan Sea in regions that produced high ice crystal concentrations (Takahashi 1993). These observations led to a physical experiment by Takahashi et al. (1995) in which collisions between small ice particles and large graupel were recreated. The small particles had surfaces that had grown through deposition and the large graupel had harder rimed surfaces. The hypothesized situation in which these collisions might happen is in weak updraft zones, in which large graupel particles fall onto relatively stationary small ice particles in a lower zone of the cloud. The set-up of the experiment was two ice-spheres, 1.8 cm in diameter, in a temperature-controlled cold box. One of the spheres

was kept stationary to grow by deposition and one ice sphere was rotated at 4 ms^{-1} to grow through riming. The cloud conditions in the chamber were cloud droplets with a diameter of 12 μm and 2.5 μm standard deviation. The cloud water content was kept constant at 2 gm^{-3} to achieve the same riming rate as a natural large graupel particle of 4 mm. The researchers triggered the collision by moving the rotating rod with the 'large graupel' sphere into a collision path with the stationary 'small graupel' sphere. The ejected ice particles from collisions were measured by an argon–helium laser and counted on a capture tray through a x25 magnifying glass after a 10-minute growth period. The greatest particle ejection happened at -16°C with roughly 800 splinters ejected, and the brittle deposition-grown ice branches on the stationary sphere were concluded to be the source of the fragments. The results were modelled through a simple equation (Takahashi et al. 1995):

$$P = \pi(R + r)^2(V - v)ENnN_t t \quad (1)$$

In Eq (1), *P(t)* is the production of ice particles in unit volume and time *t*. *R*, *V*, and *N* represent the radius in m, fall velocity in m/s, and number concentration of large graupel L^{-1}. The lowercase letters represent the same units for the small graupel. N_t represents the ice particle number ejected per collision and *E* stands for the collision efficiency. When these variables are estimated with the cloud measurements from Takahashi (1993) in mind the resulting value for *P* may be sufficient to explain the observations (Takahashi et al. 1995).

2.3.2 Modelling ice–ice collisions

To turn the results surrounding ice–ice collisions into theory, collisions models are mathematically described. This section will describe the two important modelling efforts in the SIP collision pathway; Vardiman (1978) and Phillips et al. (2017b). There are more modelling efforts out there, some more alike, and some more different than these two approaches. As Vardiman (1978) is the first true experiment and modelling effort into the ice-ice collision pathway it is the inspiration and should be explained as such. Phillips et al. (2017b) is one of the most recent and sophisticated modelling efforts and has shown a significant result regarding cloud ice concentration in cloud models in recent years, which will be discussed further in this section.

2.3.2.1 The original model by Vardiman

Vardiman (1978) theorised that there are two types of collisions between ice particles, or any particles for that matter, in clouds: either random collisions caused by turbulence, or ordered collisions which happen due to the different terminal velocities of the particles involved. The model Vardiman presents is for ordered collisions due to the difficulty of producing an analytically sound model for random collisions. This model, however, is claimed not to be restrictive as in non-extreme cloud circumstances the order of magnitudes of the two collision types would be roughly similar (Vardiman 1978). The main parameter of the model on ordered collisions put forward by Vardiman (1978) is the change of momentum. This parameter was chosen over the maximum force exerted and the kinetic energy of the collisions; the latter two were deemed infeasible as the maximum force exerted would depend on a coefficient of restitution that would inhabit large uncertainties. The kinetic energy would be infeasible as fracturing during the collision would render the collision inelastic due to the absorption of kinetic energy (Vardiman 1978). The fragment generation function used in the model is based on the following equations:

The equation for the conservation of momentum (Vardiman 1978):

$$\Delta M_{ijkl} = m_{ij}\left(v_{ij}^{f} - v_{ij}^{o}\right) = -m_{kl}\left(v_{kl}^{f} - v_{kl}^{o}\right) \tag{2}$$

The equation for the coefficient of restitution (Vardiman 1978):

$$e = -\frac{v_{ij}^{f} - v_{kl}^{f}}{v_{ij}^{o} - v_{kl}^{o}} \tag{3}$$

In Eqs (2) and (3), m_{ij} is the mass of the particle with crystal type *i* and size *j* in kg. The final velocity of the same particle is described by v_{ij}^{f} in m/s and the initial velocity by v_{ij}^{o} in m/s. The other particle is described by the subscripted *k* and *l*, which represent the crystal type *k* and size *l*. As momentum is conserved in this system, the change in momentum is defined as ΔM_{ijkl} in kg m/s. After solving for v_{ij}^{f} and the statistical chance for off-centre hits, the change in momentum is defined by the following equation:

$$\Delta M_{ijkl} = \frac{\pi}{4}\left\{\frac{m_{ij}m_{kl}}{m_{ij}+m_{kl}}(1+e)\left(v_{kl}-v_{ij}\right)\right\} \quad (4)$$

v_{kl}, v_{ij} here are the terminal velocities of the two particles in m/s. This all leads to the fragment generation function:

$$N_{ijkl} = x_1 + x_2 \log\left(\Delta M_{ijkl} \times 10^{-5}\right) + x_3\left(\log(\Delta M_{ijkl} \times 10^{-5})\right)^2 \quad (5)$$

The constants x_1, x_2, and x_3 are determined by the experiments through a mean square error method and N_{ijkl} is the number of fragments generated (Vardiman 1978). An overview of the resulting figures and mass-diameter relationships governing the equations can be found in Table 1. In Table 3 the resulting fragmentation functions from Vardiman (1974, 1978) can be seen with the regression (R) as measured against the observation.

Table 3. The fragmentation functions and their respective minimum momentum change values per crystal and particle type, including the R-value for the fragmentation functions respective to the experimental observations (Vardiman 1974, 1978).

Crystal type	**Minimum ΔM (kg m/s)**	**Fragmentation function**	**R**
Unrimed plane dendrite	5.59×10^{-9}	$3.234 + 0.6867\log(\Delta M \times 10^{-5})$	0.46
Lightly rimed plane dendrite	6.15×10^{-9}	$15.97 + 9.261\log(\Delta M \times 10^{-5}) + 1.432\log(\Delta M \times 10^{-5})^2$	0.60
Heavily rimed dendrite	1.36×10^{-8}	$76.36 + 49.10\log(\Delta M \times 10^{-5}) + 7.959\log(\Delta M \times 10^{-5})^2$	0.69
Lightly rimed spatial crystals	2.63×10^{-9}	$72.24 + 39.56\log(\Delta M \times 10^{-5}) + 5.521\log(\Delta M \times 10^{-5})^2$	0.80
Graupel	2.80×10^{-9}	$14.16 + 6.333\log(\Delta M \times 10^{-5}) + 0.74\log(\Delta \mathrm{M} \times 10^{-5})^2$	0.75

The analyses by Vardiman (1978) of this experiment on the crystal type and size that quantify the earlier mentioned constants in Eq (5) indicate that the degree of the rime of plate dendrites has a positive relationship with fragmentation. The heavily rimed dendritic crystals are reported to fragment the most effectively, and graupel fragments ineffectively (Vardiman 1978).

The results of the experiment indicate that the most important parameters in this system are the relative velocity and the degree of rime of the particles involved. The largest amount of fragmentation was determined to be between graupel particles and rimed crystals or dendrites. The magnitude of ice multiplication was less than a factor of 10 with every crystal combination without accretion and diffusions; with the latter two, the order of magnitude can exceed 10

(Vardiman 1978). Embedded convective clouds are estimated to have the best conditions for ice–ice collisions as a mechanism for ice concentration growth (Vardiman 1978).

2.3.2.2 Phillips formulation

The model by Phillips et al. (2017b) is the most recent and elaborated model, this model is both the inspiration and the cause of the research by the author. As the model will be used in the data analysis, described in Chapter 3, it will be discussed in length. Whereas Vardiman (1978) used the conservation of momentum as his main variable, Phillips et al. (2017b) used the collision kinetic energy (CKE) as the main parameter. The reason for choosing CKE is that total energy remains constant during any collision. This means that part of the kinetic energy within this budget will be used to create fragments, and the work necessary to create these fragments cannot be larger than the loss in kinetic energy during the collision that is not attributed to thermal energy. Phillips et al. (2017b) thus conclude that the number of fragments is an inseparable part of the energy budget and can be modelled from this input.

The restitution coefficient used by Vardiman (1978) is the classical coefficient of restitution as presented by Newton (1687), which is equal to the ratio of the relative speeds involved in the collision. This means that when the classic coefficient of restitution is used within the energy framework, the coefficient of restitution is determined by the square root of one minus the ratio of initial energy over fractional energy lost (Newton 1687). As the total energy budget also consists of stickiness and surface adhesion as well as other energy losses such as heat, noise, and inelastic deformation as breakage, an updated coefficient of restitution was necessary to exclude these effects from the coefficient.

Wall et al. (1990) provided the necessary definition of the coefficient of restitution by assuming the ratio of fractional energy lost over initial kinetic energy to be constant. The mathematical definition of the coefficient of restitution is changed so that it does not equal but rather is identical to the definition described above (Wall et al. 1990; Phillips et al. 2017b). This approach leaves room for the collision type to be incorporated into the model later. The foundation of the CKE based model was turned into a scheme for breakup in ice–ice collisions with internal constants and parameters based on the results from Vardiman (1978) and Takahashi et al. (1995). The mathematical model by Phillips et al. (2017b) is presented below:

As the model is based on the conservation of kinetic energy, the first equation of the model is the equation of the CKE (Phillips et al. 2017b):

$$K_0 = K_1 + \Delta S + K_{th} \tag{6}$$

K_0 is the initial kinetic energy, while K_1 the final energy that remains in the main particles in the system after the collision. ΔS is the surface adhesion and, lastly, K_{th} is the lost energy of the collision in the form of, for example, heat and noise. A part of the lost energy is the breakage, which is the focus of this research. The initial kinetic energy is defined as the kinetic energy of both particles involved in the collisions (Phillips et al. 2017b):

$$K_0 = \frac{1}{2}\frac{m_1 m_2}{m_1 + m_2}(v_1 - v_2)^2 \tag{7}$$

The masses of each of the two particles are represented by m_1 and m_2, and v_1 and v_2 are the velocities. The coefficient of restitution will dictate the next step in the theoretical model.
The classic definition of the coefficient of restitution by Newton (1687) in the kinetic energy framework is (Phillips et al. 2017b):

$$q = \sqrt{1 - \frac{K_{th}}{K_0}} \tag{8}$$

This definition of the coefficient of restitution works in situations where $\Delta S = 0$, as Phillips et al. (2015) showed there is some probability of stickiness involved in snow–graupel observations (Phillips et al. 2015). Thus, in the model a new definition of the coefficient of restitution was used, as proposed by Wall et al. (1990) (Phillips et al. 2017b):

$$q \equiv \sqrt{1 - \frac{K_{th}}{K_0}} \tag{9}$$

This change in definition allows the model to be used in situations where surface adhesion and stickiness might play a role in the collision dynamics (Phillips et al. 2017b). As it was shown to be constant over a wide range of velocities (Wall et al. 1990), the coefficient can be used as a constant to derive the next step in the model (Phillips et al. 2017b):

$$\delta K_{th} = b_2 K_{th} \approx b_2 K_0 (1 - q^2) \tag{10}$$

δK_{th} is the part of the lost energy that goes into breakage and fragmentation. The ratio of this energy is presented in the form of the constant b_2. Now, the energy budget available for fragmentation is defined. The next step is a fragmentation equation (Phillips et al. 2017b):

$$\mathcal{N} = \mathcal{N}_{contact} P\left(\frac{\delta K_{th}}{\mathcal{N}_{contact}} \geq G_{break}\right) \tag{11}$$

$\mathcal{N}$ is the number of fragments generated by a collision. $\mathcal{N}_{contact}$ is the number of branches or areas that are breakable in the contact zone. The second half of the equation represents the probability (P) that the amount of kinetic energy available per breakable branch exceeds the work necessary to break it (G_{break}). The number of branches that are breakable within the contact zone depends on the number density $n_{branch}(\mathbf{M})$. This value itself only counts for the area of the smallest particle that is involved in the collision (α) and the collision type ($\mathbf{M}$) (Phillips et al. 2017b). The collision type is dictated by the circumstances and historical circumstances in which the involved particles grew, such as temperature (T), relative humidity over ice (RH_i), dimension of the particles involved (D), and rimed fraction (Ψ) (Phillips et al. 2017b). The following formula results, including a fractional constant b_1:

$$\mathcal{N}_{contact}(\mathbf{M}) = \alpha b_1 n_{branch}(\mathbf{M}) \tag{12}$$

What remains is a theoretical definition of the work needed for fragmentation and the probability of this happening in the collision. In Eq (11) this is portrayed by $P(\frac{\delta K_{th}}{\mathcal{N}_{contact}} \geq G_{break})$; however, this is not yet applicable in a model. To determine the value of this, Phillips et al. (2017b) approached the problem by looking at the width of the asperities or branches and

the work necessary to break them. The width of a single asperity (Ξ) is portrayed in the model by the following exponential distribution (Phillips et al. 2017b):

$$p(\Xi) = \lambda \ \exp(-\lambda\Xi) \tag{13}$$

The slope parameter λ is calculated by 1 over the average of asperity widths and is a characteristic of the material, as work needed to break a single asperity, G_{break}, is assumed to be proportional to the cross sectional area of the asperity, or the quadrate of the width (Phillips et al. 2017b). This means that the relation between the asperity width and G_{break} can be described by the following equation, in which a constant, b_3, is added (Phillips et al. 2017b):

$$\Xi \approx b_3 G_{break}^{\gamma} \tag{14}$$

γ is assumed to be approximately ½ (Phillips et al. 2017b). Weibull distributions are often used in engineering applications to predict failure rates and breaking strengths (Phillips et al. 2017b). In this context, a Weibull distribution of the probability distribution of G_{break} is represented in the following equation (Phillips et al. 2017b):

$$g \propto G_{break}^{\gamma-1} \exp\left[-\left(\frac{G_{break}}{G_c}\right)^{\gamma}\right] \tag{15}$$

In Eq (15), G_c is the scale parameter of the Weibull distribution. The distribution provides the following mean for G_{break} (Phillips et al. 2017b):

$$\langle G_{break} \rangle = G_c \Gamma\left(1 + \frac{1}{\gamma}\right) \tag{16}$$

Here, Γ introduces the gamma function of the distribution. The new relationships of g and λ are depicted below in Eqs (17) and (18) (Phillips et al. 2017b):

$$g = p \frac{d\Xi}{dG_{break}} \tag{17}$$

$$\lambda = \frac{1}{b_3 G_{break}^{\gamma}} \tag{18}$$

Now, to create a useful equation for numerical efforts, the assumption $P\left(G_{break} \leq \frac{\delta K_{th}}{\mathcal{N}_{contact}}\right) = P(\Xi \leq \Xi_0)$, is taken. This means that the likelihood that an asperity will break can be defined by the width of said asperity and its being smaller than a certain width defined from CKE (Phillips et al. 2017b). For this to be put into the theoretical model, there must be a definition of the surviving width threshold, Ξ_0:

$$\Xi_0 = b_3\left(\frac{\delta K_{th}}{\mathcal{N}_{contact}}\right)^{\gamma} = b_3\left[\frac{b_2 K_0(1-q^2)}{\alpha b_1 n_{branch}}\right]^{\gamma} = \Omega(T, D, \psi, RH_i, \dots)\left(\frac{K_0}{\alpha}\right)^{\gamma} \tag{19}$$

In this equation $\Omega(T, D, \psi, RH_i, \dots) = b_3\left[\frac{b_2(1-q^2)}{b_1 n_{branch}}\right]^{\gamma}$. This leads to the formulation of the two probabilities in the following equation (Phillips et al. 2017b):

$$P\left(G_{break} \leq \frac{\delta K_{th}}{\mathcal{N}_{contact}}\right) = P(\Xi \leq \Xi_0) = \lambda \int_0^{\Xi_0} \exp(-\lambda \Xi) d\Xi$$
$$= 1 - \exp\left[-\lambda \Omega \left(\frac{K_0}{\alpha}\right)^{\gamma}\right] \tag{20}$$

When this is applied to the theoretical fragment generation function the following relationship is reached (Phillips et al. 2017b):

$$\mathcal{N} = \alpha A(T, D, \psi, RH_i, \dots) P\left(\frac{\delta K_{th}}{\mathcal{N}_{contact}} \geq G_{break}\right) \propto 1 - \exp\left\{-\left[\frac{C K_0}{\alpha A(T, D, \psi, RH_i, \dots)}\right]^{\gamma}\right\} \tag{21}$$

Here a morphology-dependent collision type $C(\mathbf{M})$ is introduced and $A(\mathbf{M}) = b_1 n_{branch}(\mathbf{M})$, and a coefficient of the fragility of the asperities is added in the form (Phillips et al. 2017b):

$$C = \frac{b_2(1-q^2)\Gamma\left(1+\frac{1}{\gamma}\right)}{\langle G_{break} \rangle} \tag{22}$$

This marks the finish of the theoretical breakup and fragmentation model. To apply this in actual modelling efforts certain assumptions need to be made and aspects of the theory simplified. The first is the assumption about collision morphology type **M**. In the application of the model, it was only assumed to be controlled by the contemporary temperature, dimension, and rime fraction of the particle (Phillips et al. 2017b). The value for C is thus simplified into a constant per collision type (Phillips et al. 2017b) using the following equation:

$$\mathcal{N} = \alpha A(\mathbf{M}) \left(1 - \exp\left\{-\left[\frac{CK_0}{\alpha A(\mathbf{M})}\right]^{\gamma}\right\}\right) \tag{23}$$

This leads to a bin model application of the following functions (Phillips et al. 2017b):

$$\begin{cases} \Delta N_i \approx \mathcal{N}\delta N_1 \delta N_2 \pi (r_1 + r_2)^2 |v_1 - v_2| E_c \Delta t/\rho \\ \Delta Q_i = \Delta N_i \zeta m_l \end{cases} \tag{24}$$

In Eq (24) the bin model is explained, and aspects of the model are introduced. Eq (24) shows the change in the number concentration of one of the particle types, ΔN_i, over time step Δt. E_c is the collision efficiency, and the number concentrations are represented by δN_1 and δN_2. The particles have fall speeds of v_1 and v_2 in their respective bin sizes of r_1 and r_2. This is all divided by the air density, ρ. From here the number concentration changes are used to calculate the mass mixing ratio of species receiving fragments, ΔQ_i. To get this mixing ratio the number concentration changes are multiplied by the ratio of the initial fragment mass to the parent particle mass, ζ, and the mass of the most fragile particle in the collision m_l.

The model described above depends on assumptions and on collision morphology, which makes it especially hard to use without the proper underlying data. The model is aimed to be used over the following subsets of collision types

1. graupel/hail colliding with other graupel/hail;
2. crystals or snow colliding with graupel/hail; and
3. crystals or snow colliding with other crystals or snow (Phillips et al. 2017b).

The parameters influenced by the morphology-dependent collision types are represented in Table 4 below:

Table 4. The parameters in the Phillips's break up formulation. (Phillips et al 2017b).

Parameter	**Collisions with dendrites and any ice**	**Collisions between spatial planar and any ice crystal**
$A(m^{-2})$	$(1.41 \times 10^6) \times (1 + 100\psi^2) \times (1 + \frac{3.98 \times 10^{-5}}{D_a^{1.5}})$	$(1.58 \times 10^7) \times (1 + 100\psi^2) \times (1 + \frac{1.33 \times 10^{-4}}{D_a^{1.5}})$
$C(J^{-1})$	$(3.09 \times 10^6) \times c$	$(7.08 \times 10^6) \times c$
γ	$0.50\text{-}0.25\psi$	$0.50\text{-}0.25\psi$
$\mathcal{N}_{max}$	100	100
c	3.5×10^{-3}	3.5×10^{-3}
ζ	0.001	0.001

For snow–graupel collisions the numbers presented in the table above are fitted to the results from Vardiman (1978) through a mean square error method. T asperity-fragility coefficient, *C*, is fitted similarly and its correction factor for sublimation weakening in the observations of Vardiman (1974, 1978), *c*, is taken from Takahashi et al. (1995) (Phillips et al. 2017b). The number density of asperities, *A*, is both influenced by the rime, ψ, and the diameter of the weakest particle involved in the collision, D_a. The results of the application of the model presented in this subsection will be described in the next paragraph.

2.3.2.3 Modelling results

The model that resulted from this theoretical basis and experimental data was then used in two atmospheric models to determine how it would perform in comparison to a well observed line of convective clouds close to the Kansas–Colorado state borders on the evening of 19 June 2000 (Lang et al. 2004). The two models used in the numerical simulations are the HUCM model, a two-dimensional bin microphysics model that incorporates more particle types (hail, graupel, snow, and some crystal types) (Phillips et al. 2017a); and the three-dimensional AC model, which aims to represent the coupling of aerosol chemistry with cloud microphysics. The two models were run with the Phillips et al. (2017b) ice–ice collision breakup scheme and a control run in which ice–ice collisions were neglected. The results from both these numerical experiments were compared to the observed results from the Severe Thunderstorm Electrification and Precipitation Study (Lang et al. 2004). Results showed that the ice concentration in these clouds could only be represented by incorporating the ice–ice collision

scheme into the models (Phillips et al. 2017a). When this aspect was excluded the ice concentration of particles over 0.2 mm in size in convective updrafts was low by an order of magnitude of 1 or 2 (Phillips et al. 2017a). The incorporation of ice–ice collisions in the model caused a precipitation drop of 20–40% (Phillips et al. 2017a). The main contributing collision type is the snow–graupel collision as the concentration of vapor-grown snow particles largely exceeds the graupel concentration, making these collisions the most likely. Due to the (partial) glaciation of the cloud leading to the loss of supercooled droplets, the total ice concentration of the clouds dropped by 60% as homogenous freezing was inhibited (Phillips et al. 2017a). These results emphasize the importance of snow–graupel collisions in cloud and storm behaviour.

A simplified version of the model presented in Phillips et al. (2017b) was used in the Consortium for Small Scale Modelling framework (COSMO) (Sullivan et al. 2018a). The framework already has an inbuilt system for the H-M process and now the ice-ice collision breakup scheme is added by simplifying the model of Phillips et al. (2017b) to rely solely on temperature, based upon the results by Takahashi et al. (1995) (Sullivan et al. 2018a). Besides ice-ice collisions, the SIP pathway of frozen droplet shattering was also added to the model. The two-moment physics model was then used to calculate the sensitivities of ice cloud number concentrations (ICNC) to the respective processes. The model was directed to reconstruct the narrow frontal rain clouds as observed over the UK on the 3rd of March 2009 by the Aerosol Properties, Processes and Influences on the Earth's climate, and the Chilbolton facility for atmospheric and radar research campaigns (Sullivan et al. 2018a). The results showed that when all SIP processes were combined in the model run the COSMO model did the best job in representing the observed ICNC. However, the results from the COSMO model still underestimate the ICNC when compared to the observations. The hypothesized causes are the lack of feedback mechanisms between the SIP processes and the underestimation of updrafts, the latter having strong influence on the ice-ice collisions mechanism (Sullivan et al. 2018a). The main conclusion from the results by Sullivan et al. (2018a) is that, even when simplified in the COSMO model, the ice-ice collision pathway appears to be essential to be able to better compute clouds and their characteristics and precipitation rates.

Phillips formulation of breakup due to ice-ice collisions, as described in Section 2.3.2.2, was implemented in a coupled model system by Sotiropoulou et al. (2020) and compared to

observed Arctic clouds. The cloud observations were made by airplane near Svalbard, Norway on the 13th of July 2013 between 10:00 and 11;00 UTC, in a stratocumulus cloud by the Aerosol-Cloud Coupling And Climate Interactions Arctic (ACCACIA) campaign. The INP concentrations had a maximum mean of 0.05 L^{-1} measured at -9°C, whereas the measured mean ICNC under the same conditions was 1.43 L^{-1}, with a peak at -5°C. Thus, indicating the presence of ice multiplication as the horizontal windspeeds were not strong enough to expect other ice or snow blow in from other regions. Phillips formulation was introduced to a coupling of a Langragian Parcel Model (LPM), that included the modelled versions of several SIP mechanisms, and a Large Eddy Simulation (LES) that calculates the boundary-layer conditions and thermodynamics (Sotiropoulou et al. 2020).

The two SIP mechanisms that were tested specifically were rime splintering (RS), and break-up in ice-ice collisions, the latter through Phillips formulation and the scaling of the results from Takahashi et al. (1995) as both described in Phillips et al. (2017b). The results from the study showed that when the SIP processes are combined the observed cloud conditions can be closely reproduced (Sotiropoulou et al. 2020). Possibly due to the RS process, providing ice particles and increasing ICNCs to a level that initiates the ice-ice collision mechanism, which eventually takes over in efficiency from RS (Sotiropoulou et al. 2020). In the temperature range described above (-5 to -10°C) Sotiropoulou et al. (2020) used the Phillips formulation and Takahashi scaling to set the upper limit of ice fragments produced per collision to 5. This gave a multiplication efficiency of 10.58, similarly to the multiplication efficiency in Phillips et al. (2017a) described at the start of this section. The results indicate that the ice-ice collision process is the most effective of the two SIP processes tested in the research, however, it is dependent on the splinters produced by the rime splintering process to start. As rime splintering is already introduced in many cloud models, Sotiropoulou et al. (2020) emphasize the importance of more research into ice-ice collisions.

Further research in which Phillips formulation was applied to a mesoscale model for the first time instead of to smaller models indicated a prominent role for break-up collision schemes (Sotiropoulou et al. 2021). In this research, Antarctic clouds were observed by the MAC field campaign over the Weddell Sea and its Antarctic coast in November and December 2015. The results from the modelling effort showed that fragmentation can create modelled ICNC comparable to the observed levels in clouds along the Weddell Sea's Antarctic coast, provided

that the concentration of INPs is above 0.1 L^{-1}. These realistic results only occur, however, when a sufficiently high rime fraction (0.4), compensating for the lack of a graupel species in their model, is used within Phillips formulation. The latter indicates that there needs to be a high enough concentration of supercooled droplets for the application of the fragmentation model to be realistic. It is stated that the mesoscale modelling efforts in which the fragmentation function is added has a significant effect on the radiative properties of the clouds (Sotiropoulou et al. 2021). This effect in turn has large impacts on surface ice melting, thus stressing the importance of a thorough understanding of SIP and collisional fragmentation once again.

2.4 Background overview and research aims

To conclude the current chapter a short summary of the background on snow–graupel collisions is provided here to set up the methods of this research. The ice concentration of MPCs has been shown to be an important factor in small to large-scale clouds, weather, and climate processes. The number concentration of ice particles in such clouds cannot be fully explained by the lower INP concentrations. Decades ago, these observations of low concentrations of INPs compared to ICNC led to the introduction of SIP (Hobbs 1969). Multiple SIP pathways have been identified; however, most research has only focussed on the HM mechanism of rime splintering, which takes place in a narrow temperature range and only works with droplet sizes over 24 μm. Overshadowed by the HM process are other mechanisms, one of which is fragmentation due to ice–ice collisions. Models have reported contrasting results of either a high or low potential for this pathway depending on the cloud type and only several physical experiments have been conducted into this mechanism.

Based on the experiments and modelling efforts by Vardiman (1974, 1978) and Takahashi et al. (1995) and the recent modelling effort by Phillips et al. (2017b) a large role for snow–graupel collisions is expected for ice multiplication in clouds. However, due to the limited empirical research the model is based on, Phillips formulation has a prediction error of a factor of 2 (Phillips et al. 2017b). Therefore, as mentioned in the introduction, the overall aim is to improve or validate the values and certainty of the parameters in the formulation of Phillips et al. (2017b), therefore enhancing the certainty of its predictions when applied in cloud modelling. This aim is targeted by answering two sub-questions;

1. Can the aim be achieved by incorporating previously unused studies into the fitment of the parameters in the formulation?
2. Can the aim be achieved by developing an experiment in which snow-graupel collisions are recreated in controlled conditions?

As can be seen by the two research questions there is an explorative character to the research conducted. Furthermore, does the state of science described in this chapter show limited literature in regards tot he specific subject of snow-graupel collisions, and less publications on experiments in this field.

3 Methods

Here the means, materials, and methods will be described that were used in the present study. The chapter will start with a description of the efforts to apply previous empirical observations from the literature to constrain the Phillips formulation (Chapter 2.3.2.2; Eq 23) by combining photographic and experimental evidence. The sections afterward will describe the attempts at creating artificial snow and graupel particles in the laboratory, so that their fragmentation may be observed in the laboratory in future work.

3.1 Fitting of the formulation to published lab data

Griggs and Choularton (1986) grew five types of ice crystals to the size of roughly 3 millimetres. The experiment focussed on finding minimum velocities of falling glass beads that would cause the fragmentation of the crystal, releasing only one fragment. The results of this experiment can be seen in Table 1 in Chapter 2. To use this data in the Phillips formulation of breakup in ice-ice collisions all the inputs needed to be determined: α, *A*, *C* and CKE. As the focus in the present study is on unrimed particles, and as no degree of rime can be estimated from the paper of Griggs and Choularton (1986) the degree of rime was assumed to be zero in all aspects of the handling of Griggs and Choularton (1986) data.

To be able to determine the CKE of the glass bead, a measure of its mass was necessary. The glass beads used in the experiment have a diameter of 270 μm (Griggs and Choularton 1986). Glass beads with such a small diameter are a specialized product with niche usability, one of the main uses of such beads is 'sand-blasting', stripping paint or rust from surfaces by blasting it with a stream of tiny glass beads. From industry websites, the density of glass beads in this size range is reported as 2.5×10^3 kg/m^3. Assuming the glass bead is shaped like a sphere, the mass is calculated from the volume by multiplying it by its density.

The CKE of the glass bead colliding with the fixed crystal was assumed to be: $\frac{1}{2}mv^2$, where m is the mass of the bead in kg and v its speed at impact in m/s. This can be done because the crystal particles in the set-up from Griggs and Choularton (1986) are grown on a fixed position

on a rod and have a velocity of zero during the collision. The fixed position is expressed by assuming the mass of the crystal to go to ∞ (Phillips et al. 2021).

The last parameters that were to be determined before being able to use the Phillips formulation were α and *A*. The α was determined by the smallest particle in the collision. In the case of the experiments in Griggs and Choularton (1986) it is the spherical area of the glass bead. The parameter *A* was determined by the weakest particle; in the case of the experiments by Griggs and Choularton (1986) these are determined from the crystal sizes. Now all parameters and inputs were in place to check the output of the fragmentation function in Eq (23). The original scheme with different versions of the asperity fragility coefficient all predicted fragmentation of <1. This is due to the original scheme returning $\alpha \times A < 1$. Hence, Eq (23) can never exceed this value.

Solving the fragmentation function for unity using the input from the collisions described in Griggs and Choularton (1986) returns new values of *A* for the crystal types and the sizes described previously. This process was done for three values of the asperity fragility coefficient (*C*) as seen in Eq (23). The values are from the original function excluding and including the correction factor for sublimation weakening, and new experimental values found by (Gautam 2022), respectively 3.09×10^6, 1.08×10^4, and 3.86×10^4 J^{-1}. When extrapolating the resulting functions by changing the CKE through increasing or decreasing the velocity of the glass bead, returns the lines as seen in Figure 1 in the results chapter.

To improve the application of the Phillips formulation to the experiments described in Griggs and Choularton (1986) there are three parameters that can be changed in Eq (23). *A*, *C* and the shape parameter, γ. The fitting process of the formulation to the data from Griggs and Choularton (1986) is described in the following four steps.

Step 1: Inspection of literature of ice morphology observations

The first step was to check existing literature whether there were any basic assumptions that could be made about the five different ice crystal morphologies observed by Griggs and Choularton (1986). Several assumptions were derived from descriptive and photographic evidence presented by Bailey and Hallett (2009), Vardiman (1974), Griggs and Choularton (1986), Comola et al. (2017), Pruppacher et al. (1997), and Schwarzenboeck et al. (2009).

Schwarzenboeck et al. (2009) and Comola et al. (2017) focused on photographic, observational and modelling evidence to determine the locations at which crystals break and from these the breakable asperities and branches were estimated for dendrites and broad branched / planar particles. These assumptions were compared to the temperature ranges of crystal growth in the classification tables from Pruppacher and Klett (1997) and Bailey and Hallett (2009) to check whether the temperatures and produced crystals overlap.

From the inspection of the literature of ice morphology observations, the assumptions were drawn that the asperity width, thickness and the total number of asperities could be determined. The number of asperities assumed per crystal type are thought of as an absolute maximum, meaning that if CKE would be increased, there would be no more additional fragments produced. This maximum is assumed for 3 mm sized particles as grown by Griggs and Choularton (1986). Furthermore, it was assumed for 3 mm sized particles that there are stable ratios for which A can be determined from the dendritic parameter across the other four morphologies.

Step 2: Modify form of A in formulation

From the data presented in Figure 1, and the accompanied values of *A* in the original scheme to produce these results, it was assumed that a new definition of *A* is required. The original scheme in Phillips et al. (2017b) defines *A*, the number density of asperities per m^2, for dendritic crystals as:

$$A = (1.41 \times 10^6) \times (1 + 100\psi^2) \times \left(1 + \frac{3.98 \times 10^{-5}}{D_a^{1.5}}\right) \quad (25)$$

However, in the current experiment no dependence of rime was assumed due to the observations and limited reporting regarding degree of rime in Griggs and Choularton (1986). Thus, ψ in Eq (25) was considered to be zero. This leaves the value of *A* to be determined by the pre-factor, 1.41×10^6 m^{-2}, and the diameter dependent part of the equation, $(1 + \frac{3.98 \times 10^{-5}}{D_a^{1.5}})$.

As the original scheme was determined through larger datasets, the original scheme is assumed to have the correct relationship between the diameter and number density of asperities.

Therefore, only the pre-factor, defined as *Y* in Eq (26), was altered to fit the data described in Griggs and Choularton (1986).

$$A = Y \times \left(1 + \frac{3.98 \times 10^{-5}}{D_a^{1.5}}\right) \tag{26}$$

By assuming the stable ratios between crystal morphologies at equal sizes, it means that for equal sizes the value of *A* can be taken by multiplying the pre-factor *Y* by the determined ratio. Hence, by determining the value of the pre-factor for unrimed dendritic crystals, the values of *A* for the other four morphologies can be determined.

Step 3: Establishment of control ratios for LSE testing and fitting

The input data provided by Griggs and Choularton (1986) for this experiment gave the sizes of the particles involved. The CKE in their experiment has been determined from the description and reported velocity and the observed fragmentation for all crystal morphologies is 1 fragment per collision of the glass bead with the fixed crystal. G_{break} , as stated in Chapter 2 and by Phillips et al. (2017b), is assumed to be proportional to the cross-sectional area of the asperity. As shown in Eq (22), the asperity-fragility coefficient (*C*) is defined as proportional to the average work required to break the asperities in a particle, $\langle G_{break} \rangle$. The absolute values of the asperity-fragility coefficients for different morphologies could not be determined from the photographic evidence, however, their relative strengths could be determined from the widths of expected asperities and their thickness. The width is measured from the previously mentioned photographic evidence and Griggs and Choularton (1986), and the thickness was derived from the classification tables in Pruppacher and Klett (1997).

The ratios taken from the estimated cross-sectional area of the breakable asperity were used to check the outcome of the fitting of the scheme, as elaborated in Step 4. The established ratios for the density of the number of asperities (*A*) and asperity-fragility coefficients (*C*) can be seen in Table 5.

Table 5. The estimated ratios of asperity-fragility coefficients, C, and number density of asperities, A. All estimated ratios are accounted for particle sizes of 3 millimetres. By being ratios, the numbers are by nature unitless.

Crystal type ratio	**Ratio of** C	**Ratio of** A
Dendrite/ Dendrite	1	1
Needle/ Dendrite	3.73	0.167
Prisms/ Dendrite	7.58	0.167
Broad/sector branched (>-12 °C)/ Dendrite	1.05	0.333
Broad/sector branched (<-16 °C)/ Dendrite	1.05	0.333

Step 4: LSE fitting procedure

With all the input parameters and assumptions in place, the data from Griggs and Choularton (1986) was used to find an updated scheme of Phillips formulation that encompasses the five described morphologies.

The experiment by Griggs and Choularton (1986) was simulated with the formulation for all five crystal types. This involved solving the Phillips formulation for a fragment number of unity for each crystal type, given the trial value of A. That trial value was inferred for each crystal type from the trial value of A for the dendritic crystal in the experiment through the ratios presented in Table 5. A loop over a wide range of possible trial values of Y for dendrites and γ (assumed to have the same value for all five types) yielded these corresponding trial values of A. The values of Y adhered to the rule that αA is larger than 1 for all crystal types, as this is the minimal requirement to determine the minimal value of Y through the observations of Griggs and Choularton (1986). The sum of the squares of the errors was used as a metric for the predicted and estimated ratios of C. The shape parameter, γ, was varied in the range 0.01 to 0.50 to find the value of parameters that produced the lowest sum square error. For each set of trial values of Y, A and , γ comparison between the predicted and estimated (Step 3, Table 5) values of the ratios of C allowed the optimum combination of values to be found.

Comparison to previous observations

The resulting scheme was compared to the lab/field observations of dendritic snow and broad-branched / planar crystals by Vardiman (1974, 1978). To be able to compare this data, the scheme needed to be adapted to the collision circumstances in the experiment by Vardiman (1974). The observed mass-diameter and velocity-diameter relationships were given by Vardiman (1974), as well as the formula of the delta momentum equation in collision with a fixed plate:

$$dM = m_{ij} v_{ij} (1 + e).$$

Vardiman (1974) describes finding a coefficient of restitution, *e*, of 0.37 for graupel collisions with a fixed plate and states this value has been used for the other particles as their values for *e* were unable to obtain properly. The momentum change and the collision kinetic energy were then calculated by using the reported relations of diameter with either mass or velocity by Vardiman (1974, 1978) across a range of diameters from 0.5×10^{-3} to 5×10^{-3} m.

The same diameters were used to calculate the value for *A*. The last unknown parameter, α, is the equivalent spherical area of the particle. In the case of collisions involving the glass bead, the diameter of the glass bead was used to calculate α. In the case where snow or graupel particles were the smallest particle involved in the collision, α was calculated by determining the volume of the equivalent spherical particle through its bulk density and mass, as found in Pruppacher and Klett (1997). From the volume of the equivalent spherical particle, a diameter was found (D_s) and used in the calculation of the equivalent spherical area, α.

Upon further research of the Vardiman (1974) experiment description, it was noticed that the unrimed dendritic crystals fell on a 1 mm mesh instead of on a plate, meaning a significant reduction of the contact area and thus contacted branches. To account for this effect, the newly found scheme was implemented with a factor that multiplies the diameter of the equivalent spherical particle of the crystal by 0.23. The latter is the fraction of surface area of the mesh that consists of wire instead of open air.

3.2 Experimental set-ups and attempts

To conduct an experiment to observe collisions of either crystals or snow with graupel, the particles need to be grown in a controlled environment. For ice crystals to form, that environment must have a relative humidity over ice of over 100%, only then the water vapour present will crystallize. Different conditions account for any graupel particle, which is a heavily rimed particle (mass rime fraction over 0.5), and thus require supercooled droplets to encounter an existing particle to rime on its surface.

Graupel formation

The experimental chamber consisted of a plexiglass cylinder with internal measurements of; diameter 29 cm and height 30 cm. The flat top of the cylinder could be taken off to place or reach any equipment inside the chamber. To create graupel a cloud of droplets was inserted into a chamber by means of an ultrasonic humidifier, with a measured flow of ~85ml per hour, located in a basin of liquid water inside of the cylinder. The droplet sizes of an ultrasonic humidifier are around 1-2 microns (Kooij et al. 2019, Rodes et al. 1990). A small fan was used to spread this cloud through the chamber and ensure consistent conditions throughout the entire chamber. The chamber and equipment inside were placed inside an open-top freezer for easy accessibility. The open-top freezer would be installed to temperatures ranging from -40 to -20°C to ensure that during the frequent opening of the freezer and handling of equipment inside the chamber the temperature inside the chamber would be below -15°C. The temperature and relative humidity were measured with a combined meters that showed the values on a LED display and were placed inside the chamber. Frozen droplets, of ~1mm in diameter, positioned at the end of a thread were then spun through the cloud by means of the electric motor at 600 rpm, so that the cloud droplets would collide with the small frozen droplet and rime onto its surface, creating a graupel particle. The velocity of the frozen droplet was controlled with the length of the thread attached to the motor, in the experiment this was ~6 cm giving a velocity of ~3.8 m/s to the graupel particle. This is within the observed fall velocities of graupel particles (Takahashi et al. 1995, Yau and Rogers 1996) The velocity in combination with the concentration and size of droplets in the chamber dictates the growth rate of the graupel particle. These factors have a strong influence on the rate of successful collisions between the frozen droplet and cloud droplets. An overview of the experimental set-up is shown in Figure 2 below. Due to the transparent nature of the Perspex chamber, the growth and size of the graupel particles could be observed by opening the freezer. However, to create pictures or see the particles up close the chamber had to be opened to analyse the resulting particles. The experiment was repeated around 30 times. Resulting particles were analysed by iPhone XS 12 megapixel camera and by the naked eye.

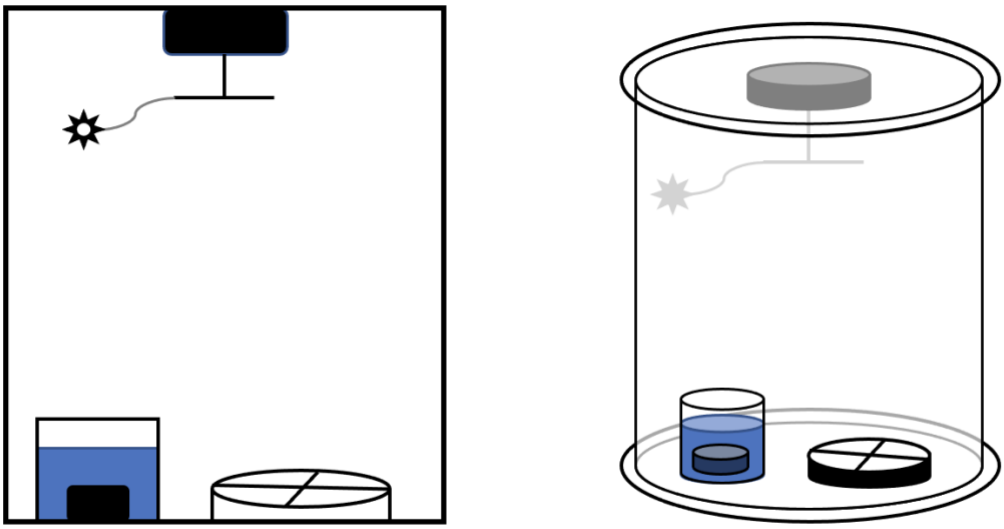

Figure 1. The two pictures portray the same experimental chamber, as used in the experimental set up to create graupel. On the left it shows a schematic view of the equipment and the cylinder, on the right a 3d render of what it looks like. On the bottom the of the chamber two of the described apparatus can be seen. The ultrasonic humidifier placed in an open top container of water on the lower left of both pictures, and a fan to disperse the cloud through the chamber. In the centre top of the two figure the electric motor with hanging particle (start shaped in the figure) can be seen.

Snow and ice crystals formation

The method to grow ice crystals involved suspending a nylon thread of diameter 0.3 mm through the centre of an ordinary 1L sized plastic soda bottle. The soda bottle had a cut-off bottom, at 3-4 cm, which could be removed and placed back, enabling opening, and closing the bottle at its widest point. The removable bottom was then entirely filled with a moist sponge at room temperature, kept in place with needles. The bottle was then placed into a 5L bucket cap down, and covered with dry ice up to two thirds of the length of the bottle. The bottom of the bottle, sticking out of the dry ice towards the ceiling, was at the same temperature as the environment. Figure 3 gives an overview of the set-up used in the alternative method described here.

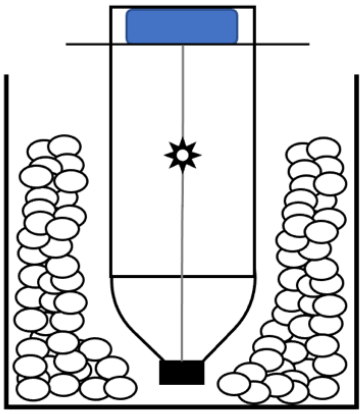

Figure 2. The alternative crystal growth method is shown. The figure shows the bottle with the cap phasing downwards in a bucket filled with dry ice. In the top of the figure, or the bottom of the bottle a blue rounded rectangle depicts the moist sponge which is exposed to the temperature of the surroundings. Along the vertical thread a crystal forms, in the figure depicted by a star shape.

During the experiment, several surrounding temperatures were used, ranging from room temperature around 20°C down to -20°C in the freezer. As the other side of the bottle was stuck in the dry ice, which has a temperature of -74°C, a steep temperature gradient forms throughout the bottle although it could not be measured due to the fragility of the set up and size of the available equipment to measure temperature. The relatively warm and moist sponge creates water-vapour saturation inside the bottle. The vapour then crystallizes onto the thread at a certain optimum location where the temperature is around -15°C indicated by the targeted dendritic crystal growth regime. This experiment was tested and tried 15 times, less frequent than the graupel methods due to the fact dry ice is not easy to come by. Resulting particles were analysed by iPhone XS 12 megapixel camera and by the naked eye.

4 Results

The following chapter will describe the results and observations of the methods described in the previous chapter. First it will start with the results of the fitting of the formulation to the data presented by Griggs and Choularton (1986). Afterwards it will continue with a description of the observations and results from the experimental attempts.

4.1 Resulting formulation after fitting published data

Initially using the data presented by Griggs and Choularton (1986) regarding dendritic crystals and fitting for a fixed value of *A* produced figure 1 below. It can be seen that when fitted simply, the results by Griggs and Choularton (1986) indicate a fragmentation rate of 2 magnitudes higher than Phillips et al. (2017b). The lines in Figure 1 indicate that the function requires a broader fitting of the parameters to the Griggs and Choularton (1986) data to make the scheme more reliable and applicable to the other crystals.

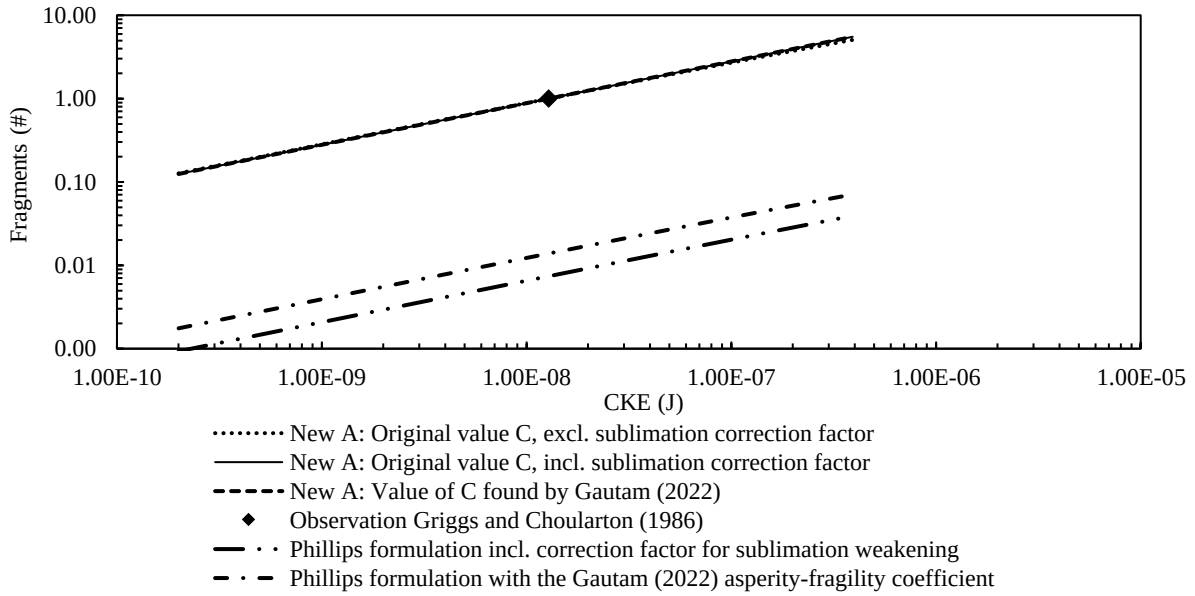

Figure 3. The observed collision between a 3mm unrimed dendritic crystal in fixed position and a glass bead of 270 μm is shown by the diamond marker. The formulations are applied to the observation by extrapolating the CKE values. The Phillips' formulation with three different asperity-fragility coefficients can be seen by the lower three lines in the figure and legend. The values of the asperity-fragility coefficient are from the original scheme including and excluding the correction factor for sublimation weakening, and the value found by Gautam (2022). The schemes with these coefficients were solved for the parameter A, against the singular observation point of the collision by Griggs and Choularton (1986). The resulting schemes are mostly overlapping in the plot and portrayed by the lines called "New A:…" in the legend, which can be seen as the upper cluster of three lines going through the marker of the observation point by Griggs and Choularton (1986).

The fitting of the Phillips formulation to the data presented by Griggs and Choularton (1986) was done by altering the pre-factor Y in Eq (26) for the number density of asperities for all crystal types at once through the estimated ratios as described in Chapter 3, step 3 and shown in Table 5. The scheme was fitted for varying values of A and γ through a least square error method. As the scheme was solved for the values of C there are three main results. The value of γ, is 0.24. The values of C and Y can be found in Table 6 below. The overall sum squared error of the results is 0.0463.

Table 6. An overview of the results with the lowest sum square error (0.0463) when fitting the Griggs and Choularton (1986) data to the Phillips formulation. The accompanied value of the shape factor γ is 0.24.

Crystal type	C (J^{-1})	Y (m^{-2})
Dendrite	1.15×10^3	1.2×10^8
Needle	1.88×10^4	2.0×10^7
Prisms	1.31×10^4	2.0×10^7
Broad/sector branched (>-12°C)	1.18×10^3	4.0×10^7
Broad/sector branched (<-16°C)	2.66×10^3	4.0×10^7

Plotting the new formulation with the updated parameters was done in multiple ways. Firstly, the collisions tested in Griggs and Choularton (1986) were extrapolated along the CKE of the glass bead by changing the velocity of the bead and keeping all other parameters similar. The resulting plots of the formulation with updated parameters are seen in Figure 4. Dendrites indeed give the highest number of fragmentation where the other lines remain relatively clustered together. The plots for prisms and needles follow each other closely.

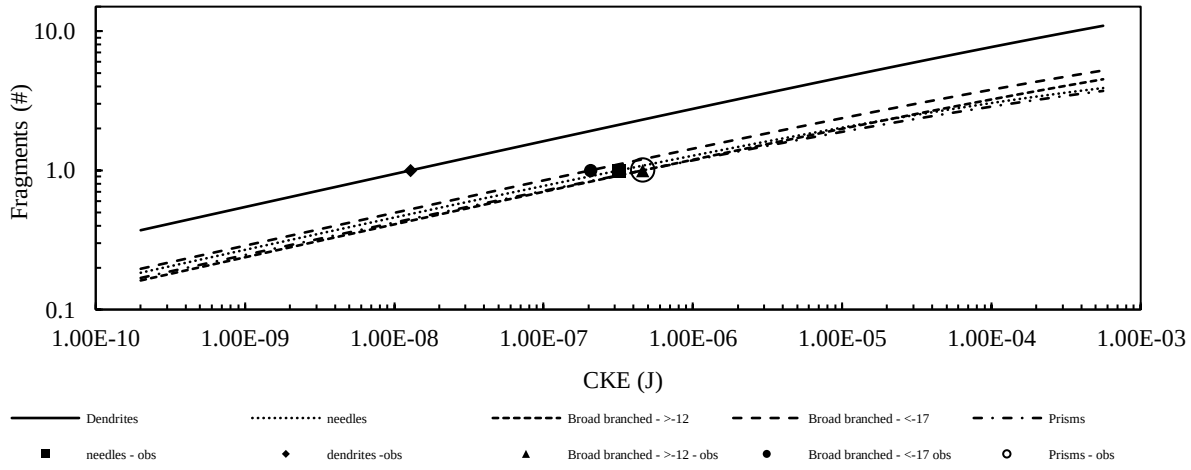

Figure 4. Collisions between 3mm sized particles fixed on a rod and glass beads of 270 μm diameter. The observations of said collisions are depicted by the singular markers. The lines show the plots of the updated formulation as described in this research. The only change in input is the CKE, which was conducted by numerically changing the velocity of the bead.

Plots of Weibull distributions follow a tilted S-shaped curve, where the start of the is down to the left. From Figure 4, the extrapolation of the scheme through the CKE of the glass beads show that the plots have not reached their maximums, indicating that the distribution can be used along other circumstances without much limitation. To compare the newly updated scheme to the results by Vardiman (1974, 1978) and the original scheme by Phillips et al. (2017b) the new scheme used Vardiman's mass-diameter relationship for the CKE, the accompanied diameter dictated the input for *A*, and the equivalent spherical area for, α. The resulting plot for dendrites can be seen in Figure 5.

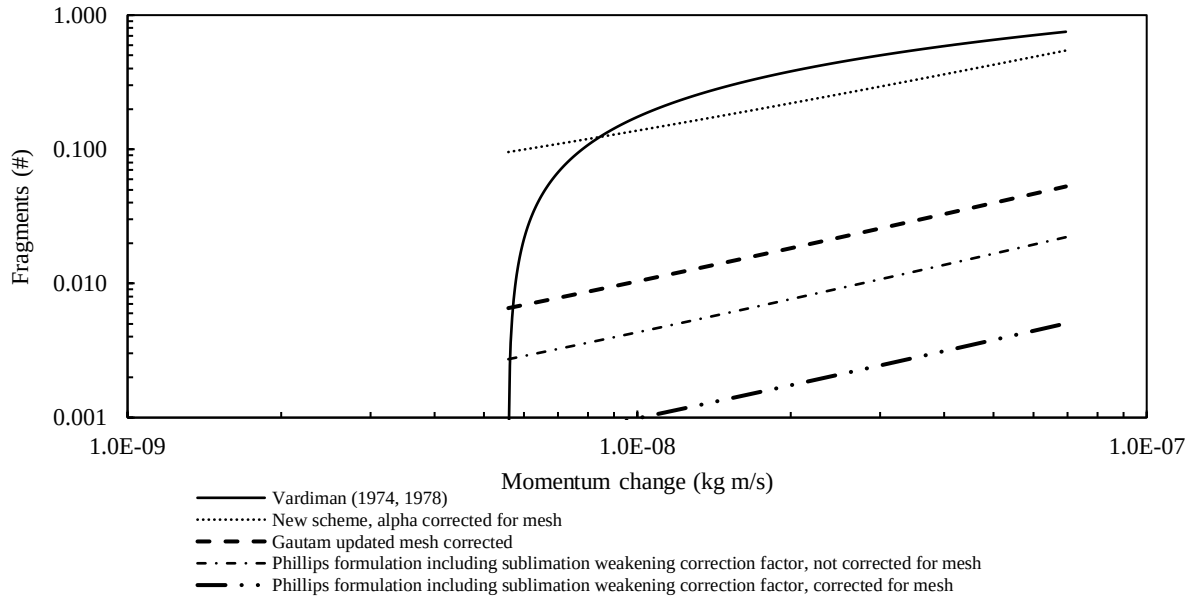

Figure 5. Plots for unrimed dendritic crystals colliding with a 1-mm copper mesh as observed by Vardiman (1974, 1978). Vardiman (1974, 1978) fragmentation scheme for unrimed dendritic crystals in the unbroken line. The scheme by Phillips et al. (2017b) is shown uncorrected for α by the short dash-dot line, and corrected by longh dash-double dot. Gautam (2022) is shown corrected for the mesh in the dashed line. The updated and resulting scheme of the present study is shown by the dotted line, correction factor for collision with mesh included in α.

The unrimed dendrites falling on top of the mesh do not carry sufficient CKE in the size range determined by Phillips et al. (2017b) to fragment themselves. It can be seen that the observed correlation between momentum change and fragmentation, the solid line by Vardiman, is higher than the new scheme, which in turn is higher than the original scheme by Phillips et al. (2017b), and significantly higher when the original scheme is corrected for the mesh.

Similar results can be seen when the broad/plate like branched crystals are plotted in the Vardiman scheme in comparison to spatial planar particles. This comparison is assumed to be correct as these particles fall into the same growth circumstances to form the spatial and planar characteristics (Bailey and Hallett 2009). The plots can be seen in Figure 6 below.

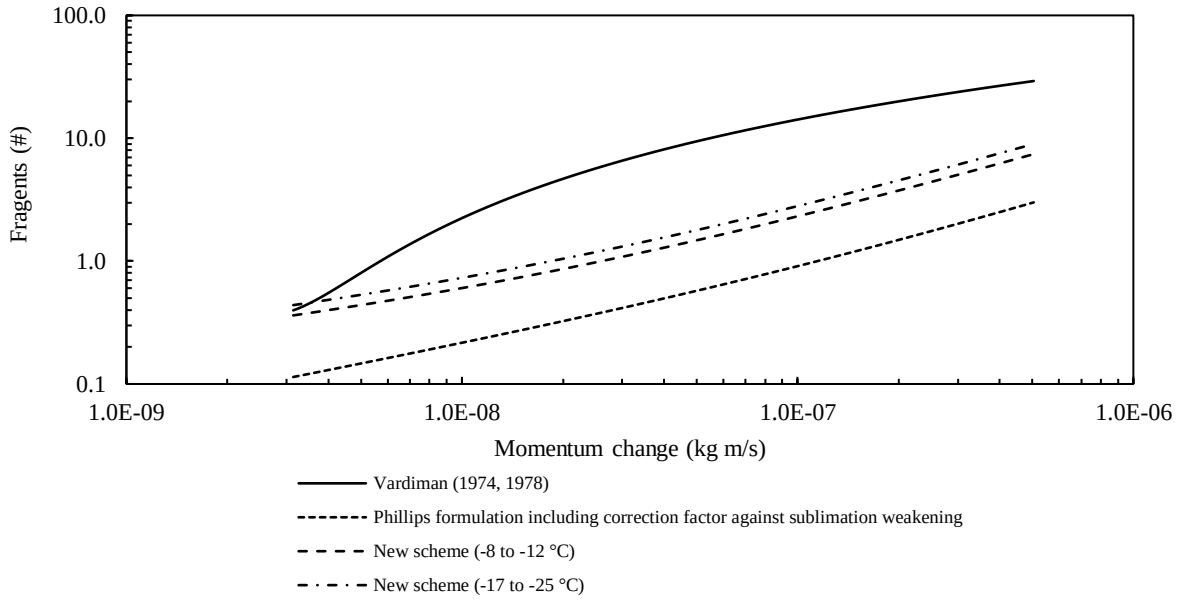

Figure 6. Collision between broad branches / planar crystals with a plate, crystal sizes in the range 0.5-5mm. Observations of lightly rimed crystals by Vardiman (1974, 1978) portrayed in the solid line. Phillips formulation is taken from Phillips et al. (2017b) and used for lightly rimed crystals. The new scheme is portrayed in the two temperature ranges observed and tested by Griggs and Choularton (1986) and is not dependent on degree of rime, between -8 and -12°C, and between -17 to -25°C.

The results from the new scheme derived from the data by Griggs and Choularton (1986) underrepresent the observation by Vardiman (1974, 1978) which can be attributed to several possible reasons, which will be elaborated in Chapter 5. The two temperature ranges of the new scheme follow each other closely and predict higher fragmentation than the Phillips formulation from Phillips et al. (2017b) including the correction factor for sublimation weakening.

Summary of results per morphology type:

i) Needles: the needle snow crystal morphology forms in the relative warmest temperature range, -4 to -6°C. No other observed data nor schemes exist for this crystal type, and thus direct quantitative comparisons cannot be made. The entirely new formulation for this crystal type found a pre-factor (Y) for the number density of breakable asperities (*A*) of 2.0×10^7 m^{-2} and an asperity-fragility coefficient (*C*) of 1.88×10^4 J^{-1}.

ii) Prisms: prisms are comparable to needles but form at slightly colder temperatures, -6 to -9°C. The results are similar to the results from needles for the number density of breakable asperities (*A)*, however, the asperity-fragility coefficient (*C*) is 31%

lower at 1.31×10^4 J^{-1}. Again, no other observed data nor schemes exist for this crystal type and thus direct quantitative comparisons cannot be made.

iii) Broad branched/ planar crystals: the resulting parameters from this research predict higher fragmentation than the Phillips et al. (2017b) formulation for snow-graupel collisions, including the correction factor against sublimation weakening. The predicted fragmentation by the newly found formulation is higher by a factor of at least 2.5 when compared to Phillips formulation including the correction factor for sublimation weakening in the simulations of observations by Vardiman (1974, 1978).

iv) Dendritic crystals: Unrimed dendritic crystals were observed by Vardiman (1974, 1978) and thus a direct comparison to the resulting scheme from this research. As seen in Figure 5, the observations of Vardiman (1974, 1978) are higher than the predictions made by the resulting scheme. The newly found parameters predict higher fragmentation for unrimed dendritic crystals when compared to the original Phillips formulation, both including and excluding the correction factor for sublimation weakening. The newly found formulation predicts higher fragmentation by at least a factor of 24 than the original formulation with the correction factor in the simulations of the observations by Vardiman (1974, 1978). Once the original formulation is corrected for the mesh this factor grows to at least about 100, as is also true for the new version of the formulation by Gautam (2022) for dendritic aggregates.

v) Broad branched/ planar crystals: this category is the same as the one in point iii above. The difference is that this category has formed in the temperature range from -17 to -25°C. The fragmentation results are slightly higher, indicating slightly higher fragmentation of this crystal morphology type at colder temperatures. When compared to the original Phillips formulation including the correction factor for sublimation weakening in the simulations of Vardiman's (1974, 1978) observations of lightly rimed spatial planar crystals, the newly found formulation predicts a higher fragmentation by a factor of approximately 3.

4.2 Products from experimental attempts

In Figure 7 the graupel particles that were successfully produced by the described methods. The 30 times the experiment has been attempted were not always successful, 14 graupel particles have been created, however, these were well conservable in the freezer. The elongated shape could be modified by cutting it in half. In figure 7 the resulting graupel particles are visible. Both of these particles grew to this size after roughly 45 minutes.

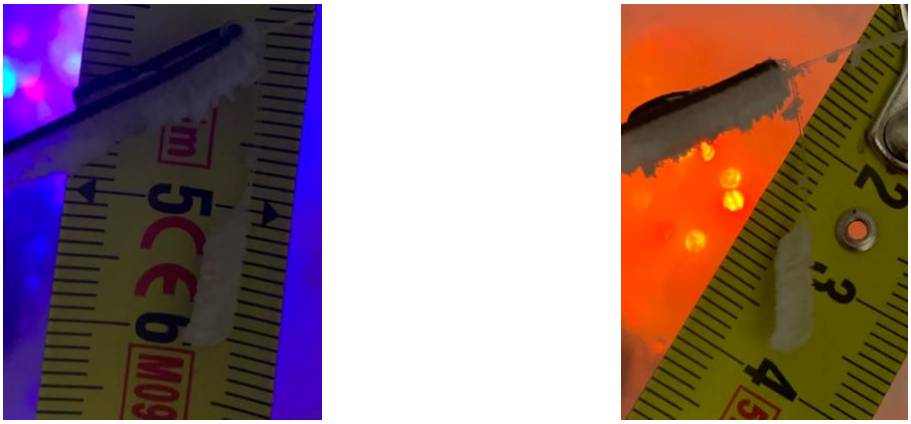

Figure 7. Both pictures show graupel particles on a thread as grown along the methods described in Chapter 3. The time to grow to this size is around 45 minutes.

The snow crystals created in the bottle are shown in Figure 8 are more like frost than snow, however this technicality can be overlooked, due to the frost being alike the arms of a dendritic crystal.

Figure 8. Resulting ice particles from the bottle in dry ice. The branches in the picture on the left have a total width of 1.5 cm +/- 20% and have formed over 50 minutes. The dendritic structures with the clear 60-degree angle between the stem and branches are visible.

The resulting crystals are a mix of fishbone like structures that form around -5°C and dendritic structures placed lower on the thread that form around -15°C (Bailey and Hallett 2009). This method is fragile, however, repeatable as 11 out of 15 attempts were successful.

After the creation of the particles any disturbance of the set-up of the methods was observed to be detrimental to the particles as these would either appear to melt or sublimate. Crystals as large as 1.5 cm would grow in 50 minutes.

5 Discussion

In the following section, the outcomes of the research into Phillips formulation and the experimental attempts will be analysed and discussed. The first section will dive into Phillips formulation and the new scheme for different crystal types. These will be infused with the results from the implementation of the Griggs and Choularton (1986) paper. The second section will dive into the attempts at developing the physical experiments and the apparent liabilities and necessary improvements for future experimental research.

5.1 Phillips formulation and newly fitted scheme

Importance of scale of predicted fragmentation

The Phillips formulation is based upon classical mechanics, statistical physics and material science (Phillips et al. 2021). The formulation of the fragmentation function is the use of two distributions, as described in Chapter 2, applied to the fragmentation caused by ice-ice collisions in clouds. Weibull distributions are often used for failure or breakage in a plethora of fields, from product and material development to systems monitoring. The way that the distributions are implemented, or better stated the way the fragmentation function works, is that the total number of breakable asperities involved in the collision are multiplied by the probability that these will break due to the collision kinetic energy. This is visible in the αA (total number of breakable asperities in collision area) and the probability part of Eq (23); $\left(1-\exp\left\{-\left[\frac{CK_0}{\alpha A(\mathbf{M})}\right]^{\gamma}\right\}\right)$.

The parameters in the fragmentation function are theoretically derived. The values of the parameters are derived from Vardiman (1974, 1978) and Takahashi et al. (1995). The versatility of the model, and its framework, is used through adapting the parameters to empirical research. The theoretical fragmentation function uses the inputs CKE, particle size, and morphology of the particles involved (Phillips et al. 2017b; Phillips et al. 2021). The morphology of the particles, determined by the atmospheric and cloud conditions during their growth, are where the uncertainties and possible inaccuracies towards the predicted number of fragments originate. The limited empirical research has provided small datasets to which the fragmentation function can be fitted.

Before any further discussion on the uncertainty and accuracy of the fragmentation function, the use of its output will be put in perspective. As described in Chapter 2, Sotiropoulou et al. (2020) put the upper limit of fragments produced per collision at $N=5$, achieving an ice multiplication factor of 10.58. An ice multiplication factor > 1 means explosive ice concentration growth until it is stopped by water sub-saturation in the cloud (Yano and Phillips 2011). Thus, even with limited fragmentation, an explosive growth in ice concentration can be expected to be caused by collisional break up. In Eq (24) it can be seen that the number of fragments stemming from the collision has a linear impact on the ice particle concentration, however its order of magnitude is more important to the overall rate of explosive ice growth rather than its specific value (Yano and Phillips 2011; Phillips et al. 2021). Therefore, it can be stated that the limited empirical evidence behind the derivations of the parameters in Phillips formulation affects its accuracy and uncertainty, however, it does not diminish the importance and relevance of the inclusion of the scheme.

Results from the fitting of the published literature data

The origin of the Phillips formulation being in existing theory makes it adaptable to fit to newly found empirical data. The fit to the experimental data by Griggs and Choularton (1986) is accompanied by estimates from observed natural snow crystals and snow crystals grown in controlled circumstances. These estimates, together with the reporting by Griggs and Choularton (1986) on the temperatures used for the crystals, allowed for the thought-experiment to extrapolate the formulation across a temperature range from -3 to -25°C. For within the range the crystal type differs depending on the specific temperature, the thought-experiment allowed the scheme to envelop a more precise morphology dependent approach.

From Figure 4 it becomes clear that dendrites remain the largest possible source of fragmentation. However, these crystals are present in a narrow temperature band and a significant increase in broad branched, or planar, crystals between the original Phillips formulation and the updated scheme can be seen in Figure 6. This widens the temperature range of possibly significant in-cloud fragmentation due to collisions. The new scheme underestimates the observed results from Vardiman (1974, 1978) both for the unrimed dendrites and lightly rimed planar crystals. This can have several possible explanations; the particles observed by Vardiman (1974, 1978) could have been crystal aggregates which are

expected to be weaker, thus enhancing fragmentation. Other reasons could be sublimation weakening indeed, or experimental differences between the two sources.

Griggs and Choularton (1986) reported that light riming of particles caused no observable difference in the breaking velocity of the glass bead. Therefore, the thought experiment of the fitting of the Phillips formulation in the present study to the observations by Griggs and Choularton (1986) excluded a possible dependence on rime. This was because the rime degrees were not quantified in the report by Griggs and Choularton (1986) and could not be estimated or safely assumed. Therefore, there might still be a positive effect of rime degree on breakage and fragmentation, however, this would require additional empirical evidence to be incorporated into the new scheme. Interestingly, in Figure 6 the new scheme is used for unrimed particles whereas the original scheme and Vardiman's observed fragmentation portray lightly rimed particles. If rime degree were indeed to play a role in fragmentation, as originally hypothesized and still thought of as highly likely, this could enhance the already higher predicted fragmentation.

Regarding point (iv) in the summary of the results in section 4.1, the numbers of fragments predicted by the new scheme in the present study are much higher than predicted either by the original formulation or by Gautam's new formulation, for the following possible reasons. First, the glass bead (0.3 mm) of Griggs and Choularton (1986) was much smaller than sizes of typical graupel (> 1 mm), and in the experiment may have concentrated the CKE in a small area, with more impact force and pressure. The impact speed of the glass bead (1 m/s) was similarly higher than fall speeds of most graupel particles. Second, the original formulation by Phillips et al. (2017b) fitted the parameters of the formulation for dendritic crystals across various mass rime fractions to the observations by Vardiman (1974, 1978). This procedure assumed that the particles fell onto a plate instead of a mesh and thus for unrimed dendrites specifically the original formulation might underestimate the fragmentation when corrected for the mesh. Third, the factor correcting for the possible weakening of the crystals caused by sublimation during the observations by Vardiman (1974, 1978) was determined from the experiments by Takahashi et al. (1995) regarding graupel and rime. The factor was extrapolated from these results to be incorporated in the crystal-graupel scheme and can be overestimated, underestimating the fragmentation from snow-graupel collisions.

The updated scheme is based on assumptions of photographic evidence and limited empirical data, consisting of 5 data points with large uncertainties. Hence, the uncertainty surrounding the scheme has not improved upon the original scheme brought forward by Phillips et al. (2017b). The thought experiment did succeed in incorporating newly found empirical evidence into the scheme in a manner based on empirical evidence rather than theory, showing the adaptability of the scheme. Furthermore, does the resulting scheme incorporate more specific crystal types and can thus be used in more detail along different cloud conditions. Future studies and experimentation can develop the parameters further and incorporate the effects of relative humidity of the air over water and ice and the mass rime degree, enhancing the accuracy of the predictions of the scheme.

5.2 Discussion of experiments and recommendations for future experimental research

Experimental attempts have successfully created graupel particles and ice crystals / snowflakes. However, as mentioned in the results these particles were not used to create any collisions. This due to the fragility of the dendritic snow crystals in the set-up. The finetuning of the methods indicated that the ways to grow these particles can be repeated with a good success rate. The slow growth rates of the particles, however, do create a time dependency. Future work to create collisional datasets such as Griggs and Choularton (1986) and Takahashi et al. (1995) need further development of these methods. The recommendation for these developments are given in chapter 6.

6 Conclusions

This research set out to test and improve the certainty and validity surrounding the parameters in the Phillips' formulation of break-up in snow-graupel collisions. The goal was targeted through two approaches; (1) finding and implementing additional empirical evidence from the literature with which to constrain the scheme to create a new version of the formulation, and (2) to develop and attempt laboratory collision experiments by creating artificial snow and graupel. The experimental approach provided the methods to create artificial snow crystals and graupel particles that can be used in possible future laboratory experiments when improved, but no observations of actual collisions were made in the present project, recommendations for future research with experimental method is provided in this chapter.

Regarding approach (1), the new version of the formulation was obtained by combining observations published by Griggs and Choularton (1986) for minimum speeds of a tiny glass bead for breaking a crystal with our own estimates from published photos of crystals for five ratios of the asperity-fragility coefficient and number density of asperities. A least squares model based on the input of number density of asperities, A, and the shape parameter, γ, was used in comparison with the independently estimated ratios of the asperity-fragility coefficient, C, values among crystal types. The resulting optimum value of the shape parameter is $\gamma = 0.24$. The resulting optimum values for the other parameters, A and C are listed in Table 6. These newfound parameters are for unrimed monomer crystals of about 5 mm in maximum dimension. Collisions involving dendritic crystals were presumed to be the most prolific, this research concludes the same, and even predicts a higher fragmentation rate of 24 to 100 times larger when compared to the original formulation by Phillips et al. (2017b).

The current approach has incorporated the effect of temperature on fragmentation, through the fact that snow crystal morphology is dependent on temperature. However, the current research has not considered the supersaturation over ice, which is the second determinant of crystal morphology. The higher the supersaturation over ice, the more branches and higher complexity the crystals will have (Libbrecht 2005; Bailey and Hallett 2009). Therefore, future research should consider the supersaturation. Another characteristic of particle morphology, the degree of rime, is not taken up into the scheme proposed in this research based on the data used.

However, as previous research has observed a dependence on rime, future research should take this into account (Vardiman 1974, 1978; Takahashi et al. 1995).

To conclude, we have inferred published photographic evidence and applied this to simulations of published fragmentation in lab experiments of collisions of glass beads with crystals from the literature. This has successfully constrained the Phillips formulation for unrimed monomer snow crystals in the temperature range from -4 to -25°C. These updated parameters allow further and more precise research of the impact of the snow-graupel collisional SIP pathway. The latter is hypothesized to have significant impacts on weather and climate modelling because the ice crystal process of precipitation production creates graupel from snow, so both are in proximity and the fragments from graupel-snow collisions can grow to form more snow (Yau and Rogers 1996), creating a positive feedback of ice multiplication in the cloud glaciation.

Recommendations for set-up of future experimental research

The growth of ice crystals should take place in the chamber where the collision will occur. This will take the weakness of the particle to thermal shock or vibrations out of the equation; therefore, a redesign of the ice crystal and snow particle chamber is necessary. The use of the steep temperature gradient due to the extreme low temperature of dry-ice and the warm saturated air has proven to be the most effective way to create large ice crystals, this should be considered when creating an upgraded snow chamber. To rime the ice crystals the growth chamber in which the ice crystal forms, needs to receive an airflow which contains a cloud of droplets and is supersaturated over ice. The snow particle itself is preferably kept in place and rotated in the air flow to create rime on all sides. The airflow should not exceed the terminal velocity values of the respective particles, or the breakage by airflow alone results presented in Griggs and Choularton (1986) and Table 1. With additional design, this chamber should be able to provide data on riming of the snow particles and graupel formation. The most effective way to instigate collisions between snow and graupel particles would be to take a graupel particle and let it fall through a tube on to the snow particle. Spinning of the graupel particle leads to multiple collisions due to the high number of rotations per minute necessary to develop adequate speeds. With a high-speed and close-up camera, measurements can be taken of the collision and fragmentation and CKE can be determined from the footage.

7 References

Avila, E. A., and R. G. Pereyra. 2000. Charge transfer during Crystal-Graupel Collisions for two different cloud droplet size distributions. *Geophysical Research Letters,* 27**:** 3837-3840. DOI: https://doi.org/10.1029/2000GL012302

Bailey, M. P., and J. Hallett. 2009. A Comprehensive Habit Diagram for Atmospheric Ice Crystals: Confirmation from the Laboratory, AIRS II, and Other Field Studies. *Journal of the Atmospheric Sciences,* 66**:** 2888-2899. DOI: 10.1175/2009JAS2883.1

Berdeklis, P., and R. List. 2001. The Ice Crystal–Graupel Collision Charging Mechanism of Thunderstorm Electrification. *Journal of the Atmospheric Sciences,* 58**:** 2751-2770. DOI: 10.1175/1520-0469(2001)058<2751:Ticgcc>2.0.Co;2

Comola, F., J. F. Kok, J. Gaume, E. Paterna, and M. Lehning. 2017. Fragmentation of wind-blown snow crystals. *Geophysical Research Letters,* 44**:** 4195-4203. DOI: https://doi.org/10.1002/2017GL073039

Deshmukh, A., V. T. J. Phillips, A. Bansemer, S. Patade, and D. Waman. 2022. New Empirical Formulation for the Sublimational Breakup of Graupel and Dendritic Snow. *Journal of the Atmospheric Sciences,* 79**:** 317-336. DOI: 10.1175/jas-d-20-0275.1

Field, P. R., R. P. Lawson, P. R. A. Brown, G. Lloyd, C. Westbrook, D. Moisseev, A. Miltenberger, A. Nenes, et al. 2017. Secondary Ice Production: Current State of the Science and Recommendations for the Future. *Meteorological Monographs,* 58**:** 7.1-7.20. DOI: 10.1175/amsmonographs-d-16-0014.1

Fuchs, B. R., S. A. Rutledge, E. C. Bruning, J. R. Pierce, J. K. Kodros, T. J. Lang, D. R. MacGorman, P. R. Krehbiel, et al. 2015. Environmental controls on storm intensity and charge structure in multiple regions of the continental United States. *Journal of Geophysical Research: Atmospheres,* 120**:** 6575-6596. DOI: https://doi.org/10.1002/2015JD023271

Gautam, M. 2022. Fragmentation in graupel snow collisions. *Master of Science dissertation, Dept of Physical Geography and Ecosystem Science, Lund University, Lund, Sweden*-. DOI: http://lup.lub.lu.se/student-papers/record/9087233

Griggs, D. J., and T. W. Choularton. 1986. A laboratory study of secondary ice particle production by the fragmentation of rime and vapour-grown ice crystals. *Quarterly Journal of the Royal Meteorological Society,* 112**:** 149-163. DOI: https://doi.org/10.1002/qj.49711247109

Guo, J., M. Deng, S. S. Lee, F. Wang, Z. Li, P. Zhai, H. Liu, W. Lv, et al. 2016. Delaying precipitation and lightning by air pollution over the Pearl River Delta. Part I: Observational analyses. *Journal of Geophysical Research: Atmospheres,* 121**:** 6472-6488. DOI: https://doi.org/10.1002/2015JD023257

Hallett, J., and S. C. Mossop. 1974. Production of secondary ice particles during the riming process. *Nature,* 249**:** 26-28. DOI: 10.1038/249026a0

Harris-Hobbs, R. L., and W. A. Cooper. 1987. Field Evidence Supporting Quantitative Predictions of Secondary Ice Production Rates. *Journal of Atmospheric Sciences,* 44**:** 1071-1082. DOI: 10.1175/1520-0469(1987)044<1071:Fesqpo>2.0.Co;2

Hobbs, P. V. 1969. Ice multiplication in clouds. *J. Atmos. Sci,* 26**:** 315-318.

IPCC. 2013. Climate Change 2013: The Physical Science Basis. Contribution of Working Group I to the Fifth Assessment Report of the Intergovernmental Panel on Climate Change. [Stocker, T.F., D. Qin, G.-K. Plattner, M. Tignor, S.K. Allen, J. Boschung, A. Nauels, Y. Xia, V. Bex and P.M. Midgley (eds.)]**:** 1535 pp.

Kanji, Z. A., L. A. Ladino, H. Wex, Y. Boose, M. Burkert-Kohn, D. J. Cziczo, and M.

Krämer. 2017. Overview of Ice Nucleating Particles. *Meteorological Monographs,* 58**:** 1.1-1.33. DOI: 10.1175/amsmonographs-d-16-0006.1

Koenig, L. R. 1963. The Glaciating Behavior of Small Cumulonimbus Clouds. *Journal of Atmospheric Sciences,* 20**:** 29-47. DOI: 10.1175/1520-0469(1963)020<0029:Tgbosc>2.0.Co;2

Kooij, S., A. Astefanei, G. L. Corthals, and D. Bonn. 2019. Size distributions of droplets produced by ultrasonic nebulizers. *Sci Rep,* 9**:** 6128. DOI: 10.1038/s41598-019-42599-8

Ladino, L. A., A. Korolev, I. Heckman, M. Wolde, A. M. Fridlind, and A. S. Ackerman. 2017. On the role of ice-nucleating aerosol in the formation of ice particles in tropical mesoscale convective systems. *Geophysical Research Letters,* 44**:** 1574-1582. DOI: https://doi.org/10.1002/2016GL072455

Lang, T. J., L. J. Miller, M. Weisman, S. A. Rutledge, L. J. Barker, V. N. Bringi, V. Chandrasekar, A. Detwiler, et al. 2004. The Severe Thunderstorm Electrification and Precipitation Study. *Bulletin of the American Meteorological Society,* 85**:** 1107-1126. DOI: 10.1175/bams-85-8-1107

Lauber, A., J. Henneberger, C. Mignani, F. Ramelli, J. T. Pasquier, J. Wieder, M. Hervo, and U. Lohmann. 2021. Continuous secondary-ice production initiated by updrafts through the melting layer in mountainous regions. *Atmos. Chem. Phys.,* 21**:** 3855-3870. DOI: 10.5194/acp-21-3855-2021

Libbrecht, K. G. 2005. The physics of snow crystals. *Reports on Progress in Physics,* 68**:** 855-895. DOI: 10.1088/0034-4885/68/4/r03

Lohmann, U., and J. Feichter. 2005. Global indirect aerosol effects: a review. *Atmos. Chem. Phys.,* 5**:** 715-737. DOI: 10.5194/acp-5-715-2005

Mignani, C., J. M. Creamean, L. Zimmermann, C. Alewell, and F. Conen. 2019. New type of evidence for secondary ice formation at around −15 °C in mixed-phase clouds. *Atmos. Chem. Phys.,* 19**:** 877-886. DOI: 10.5194/acp-19-877-2019

Mossop, S. C. 1980. The mechanism of ice splinter production during riming. *Geophysical Research Letters,* 7**:** 167-169. DOI: https://doi.org/10.1029/GL007i002p00167

Mossop, S. C. 1985. The Origin and Concentration of Ice Crystals in Clouds. *Bulletin of the American Meteorological Society,* 66**:** 264-273. DOI: 10.1175/1520-0477(1985)066<0264:Toacoi>2.0.Co;2

Newton, I. 1687. Philosophiae Naturalis Principia Naturalis Mathematica *Royal Society***:** 23.

Pattnaik, S., C. Inglish, and T. N. Krishnamurti. 2011. Influence of Rain-Rate Initialization, Cloud Microphysics, and Cloud Torques on Hurricane Intensity. *Monthly Weather Review,* 139**:** 627-649. DOI: 10.1175/2010mwr3382.1

Phillips, V. T. J., M. Formenton, A. Bansemer, I. Kudzotsa, and B. Lienert. 2015. A Parameterization of Sticking Efficiency for Collisions of Snow and Graupel with Ice Crystals: Theory and Comparison with Observations. *Journal of the Atmospheric Sciences,* 72**:** 4885-4902. DOI: 10.1175/jas-d-14-0096.1

Phillips, V. T. J., J.-I. Yano, M. Formenton, E. Ilotoviz, V. Kanawade, I. Kudzotsa, J. Sun, A. Bansemer, et al. 2017. Ice Multiplication by Breakup in Ice–Ice Collisions. Part II: Numerical Simulations. *Journal of the Atmospheric Sciences,* 74**:** 2789-2811. DOI: 10.1175/jas-d-16-0223.1

Phillips, V. T. J., J.-I. Yano, and A. Khain. 2017. Ice Multiplication by Breakup in Ice–Ice Collisions. Part I: Theoretical Formulation. *Journal of the Atmospheric Sciences,* 74**:** 1705-1719. DOI: 10.1175/jas-d-16-0224.1

Phillips, V. T. J., J. I. Yano, A. Deshmukh, and D. Waman. 2021. Comment on “Review of experimental studies of secondary ice production” by Korolev and Leisner (2020).

Atmos. Chem. Phys., 21**:** 11941-11953. DOI: 10.5194/acp-21-11941-2021
Pruppacher, H. R., J. D. Klett, and Springer. 1997. *Microphysics of Clouds and Precipitation*. Springer.
Rodes, C., T. Smith, R. Crouse, and G. Ramachandran. 1990. Measurements of the Size Distribution of Aerosols Produced by Ultrasonic Humidification. *Aerosol Science and Technology,* 13**:** 220-229. DOI: 10.1080/02786829008959440
Schwarzenboeck, A., V. Shcherbakov, R. Lefevre, J. F. Gayet, Y. Pointin, and C. Duroure. 2009. Indications for stellar-crystal fragmentation in Arctic clouds. *Atmospheric Research,* 92**:** 220-228. DOI: https://doi.org/10.1016/j.atmosres.2008.10.002
Seinfeld, J. H., C. Bretherton, K. S. Carslaw, H. Coe, P. J. DeMott, E. J. Dunlea, G. Feingold, S. Ghan, et al. 2016. Improving our fundamental understanding of the role of aerosol−cloud interactions in the climate system. *Proceedings of the National Academy of Sciences,* 113**:** 5781. DOI: 10.1073/pnas.1514043113
Sotiropoulou, G., S. Sullivan, J. Savre, G. Lloyd, T. Lachlan-Cope, A. M. L. Ekman, and A. Nenes. 2020. The impact of secondary ice production on Arctic stratocumulus. *Atmos. Chem. Phys.,* 20**:** 1301-1316. DOI: 10.5194/acp-20-1301-2020
Sotiropoulou, G., É. Vignon, G. Young, H. Morrison, S. J. O'Shea, T. Lachlan-Cope, A. Berne, and A. Nenes. 2021. Secondary ice production in summer clouds over the Antarctic coast: an underappreciated process in atmospheric models. *Atmos. Chem. Phys.,* 21**:** 755-771. DOI: 10.5194/acp-21-755-2021
Sullivan, S. C., C. Barthlott, J. Crosier, I. Zhukov, A. Nenes, and C. Hoose. 2018. The effect of secondary ice production parameterization on the simulation of a cold frontal rainband. *Atmos. Chem. Phys.,* 18**:** 16461-16480. DOI: 10.5194/acp-18-16461-2018
Sullivan, S. C., C. Hoose, A. Kiselev, T. Leisner, and A. Nenes. 2018. Initiation of secondary ice production in clouds. *Atmos. Chem. Phys.,* 18**:** 1593-1610. DOI: 10.5194/acp-18-1593-2018
Takahashi, T. 1993. High ice crystal production in winter cumuli over the Japan Sea. *Geophysical Research Letters,* 20**:** 451-454. DOI: https://doi.org/10.1029/93GL00613
Takahashi, T., and N. Fukuta. 1988. Observations of the Embryos of Graupel. *Journal of Atmospheric Sciences,* 45**:** 3288-3297. DOI: 10.1175/1520-0469(1988)045<3288:Ooteog>2.0.Co;2
Takahashi, T., Y. Nagao, and Y. Kushiyama. 1995. Possible High Ice Particle Production during Graupel–Graupel Collisions. *Journal of Atmospheric Sciences,* 52**:** 4523-4527. DOI: 10.1175/1520-0469(1995)052<4523:Phippd>2.0.Co;2
Vardiman, L. 1974. The generation of secondary ice particles in clouds by crystal–crystal collisions. *Ph.D. thesis, Colorado State University***:** 140 pp.
Vardiman, L. 1978. The Generation of Secondary Ice Particles in Clouds by Crystal–Crystal Collision. *Journal of Atmospheric Sciences,* 35**:** 2168-2180. DOI: 10.1175/1520-0469(1978)035<2168:Tgosip>2.0.Co;2
Wall, S., W. John, H.-C. Wang, and S. L. Goren. 1990. Measurements of Kinetic Energy Loss for Particles Impacting Surfaces. *Aerosol Science and Technology,* 12**:** 926-946. DOI: 10.1080/02786829008959404
Williams, E., R. Zhang, and J. Rydock. 1991. Mixed-phase microphysics and cloud electrification. *Journal of the atmospheric sciences,* 48**:** 2195-2203.
Yano, J.-I., and V. T. J. Phillips. 2011. Ice–Ice Collisions: An Ice Multiplication Process in Atmospheric Clouds. *Journal of the Atmospheric Sciences,* 68**:** 322-333. DOI: 10.1175/2010jas3607.1
Yau, M. K., and R. R. Rogers. 1996. *A short course in cloud physics*. Elsevier.

8 Appendix

8.1 Appendix A: Mathematical symbols and definitions

Symbol	Definition	Unit
A	Measure of number density of breakable asperities in region of contact	m^{-2}
b_1	Fraction of surface of smaller particle in region of impact	-
b_2	Fraction of surface of smaller particle in region of impact	-
b_3	Constant relating *J* and G_{break}	$mJ^{-\gamma}$
C	Asperity–fragility coefficient	J^{-1}
c	Correction factor for sublimation weakening	J^{-1}
D	Diameter of ice particle	m
D_a	Maximum width of smaller ice particle	m
D_s	Equivalent spherical diameter of smaller particle	m
e	Coefficient of restitution, in the scheme by Vardiman (1974, 1978)	-
E	Collision efficiency in the scheme by Takahashi et al. (1995)	-
E_c	Collision efficiency	-
$g(G_{break})$	Probability distribution function of G_{break}	J^{-1}
G_{break}	Work done to break branch or other asperity	J
G_c	Scale parameter of Weibull distribution for G_{break}	J
K_{th}	Energy lost (converted to heat, noise, and the particle's inelastic deformation)	J
K_0	Initial value of CKE	J
K_1	Final kinetic energy including CKE and any rotational kinetic energy produced	J
δK_{th}	Energy available for breaking all branches and other asperities	J
M	Vector denoting the collision type	-
m_1, m_2	Masses of colliding particles	kg
ΔM_{ijkl}	Momentum change of a collision between particles of types i and k, and sizes k and l	kg m/s
m_{ij}, m_{kl}	Masses of particles of type i and k, and sizes j and l	kg
N	Number concentration large graupel	L^{-1}
n	Number concentration small graupel	L^{-1}
n_{branch}	Number density (by surface area) of branches on smaller particles	m^{-2}
N_t	the ice particle number ejected per collision	-

Symbol	Definition	Unit
$\mathcal{N}$	Number of fragments per collision	-
$\mathcal{N}_{contact}$	Number of branches and other asperities in region of contact	-
ΔN_i	Change in number mixing ratio of species receiving fragments	kg^{-1}
$\delta N_1, \delta N_2$	Concentrations of pair of colliding particles in size ranges, (δr_1, δr_2)	m^{-3}
P	*P(t)* is the production of ice particles in unit volume and time *t*	L^{-1}
$p(\Xi)$	Probability distribution function of Ξ	m^{-1}
q	Coefficient of restitution in Phillips formulation	-
ΔQ_i	Change in mass mixing ratio of species receiving fragments	kg kg^{-1}
R	Radius of large graupel	m
r	Radius of small graupel	m
ΔS	Work done to separate particles after impact	J
Δt	Time step of atmospheric model	s
V	Fall velocity large graupel	m/s
v	Fall velocity small graupel	m/s
v_{ij}^f, v_{kl}^f	Velocity after collision of particles of types i and k, and sizes j and l	m/s
v_{ij}^o, v_{kl}^o	Velocity upon collision of particles of types i and k, and sizes j and l	m/s
v_1, v_2	Fall speeds of colliding particles	m/s
x_1, x_2, x_3	fitting parameters to Vardiman's observations	-
Y	Pre-factor in determination of *A*	m^{-2}
α	Surface area (equivalent spherical) of smaller particle	m^2
γ	shape parameter of Weibull distribution of G_{break}	-
Γ	Gamma function	-
ζ	Ratio of initial fragment mass to mass of parent particle	-
λ	Slope of probability distribution function for Ξ	m^{-1}
Ξ	Width of asperity (e.g., vapor-grown branch)	m
Ξ_0	Critical value of width Ξ corresponding to $G_{break} = \delta K_{th} / N_{contact}$ for breaking	m
ρ	Air density	kg m^{-3}
Ψ	Fraction by mass of a snow particle or crystal that is rime	-
Ω	Coefficient for the CKE-dependent threshold Ξ_0	$mkg^{-\gamma}\ s^{2\gamma}$

8.2 Appendix B: Terminology

Term	Abbreviation	Definition
Fragmentation	-	Parent particles releasing fragments of themselves after collision, the fragments are counted in fragmentation, the parent particles are not.
Glaciation (of cloud, cloud glaciation)	-	Rapid disappearance of liquid water in cloud and rapid increase in ice crystal in cloud until all particles are ice particles
Graupel	-	An ice particle in size range 0.5-5mm of which >50% of its mass consists of rime
Rime splintering, Hallett-Mossop process	HM Process	Ice splinters released during the riming process of a particle
Ice nucleating particles	INP	Particles in the atmosphere, either suspended in water or free floating upon which ice nucleates
Ice particles	-	Ice particles are any form of ice in the atmosphere, snow crystals, graupel, frozen droplets etc.
Ice-ice collisions	-	Collisions between any type of ice particles
Ice crystal number concentration	ICNC	The number of ice crystals per unit volume in the cloud
Mesoscale	-	A meteorological scale, between 10 to 10,000 km
Mixed phase clouds	MPCs	Clouds in which water consists in its liquid and frozen form
Phillips formulation	-	The formulation as published in Phillips et al. (2017b)

Term	Abbreviation	Definition
Primary ice production	PIP	The processes that create the initial presence of ice particles in the atmosphere
Radiative budget	-	The budget incoming and outcoming radiation of the Earth and its atmosphere
Secondary ice production	SIP	The processes that create ice particles from existing ice particles, i.e. through fragmentation or rime splintering.
Sublimation	-	The phase shift from solid to gaseous
Supersaturation	-	Relative humidity exceeds 100%, i.e. there is more water vapour than liquid in the air than the equilibrium prescribes
Supersaturation (over ice)	-	There is more water vapour over frozen water particles in the air than the equilibrium prescribes
Wegener–Bergeron–Findeisen process	-	Presence of water sub-saturation and ice supersaturation, fast evaporation of liquid water and fast ice particle growth through vapor deposition